Convergence of a common solution to broad ebolavirus neutralization by glycan cap directed human antibodies

Charles D. Murin[1], Pavlo Gilchuk[2], Philipp A. Ilinykh[3,4], Kai Huang[3,4], Natalia Kuzmina[3,4], Xiaoli Shen[3,4], Jessica F. Bruhn[5*], Aubrey L. Bryan[6], Edgar Davidson[6], Benjamin J. Doranz[6], Lauren E. Williamson[7], Jeffrey Copps[1], Tanwee Alkutkar[1], Andrew I. Flyak[7**], Alexander Bukreyev[3,4,8], James E. Crowe, Jr.[2,7,9], Andrew B. Ward[1,†]

[1]Department of Integrative Structural and Computational Biology, The Scripps Research Institute, La Jolla, CA, 92037, USA

[2]Vanderbilt Vaccine Center, Vanderbilt University Medical Center, Nashville, TN 37232, USA

[3]Galveston National Laboratory, Galveston, TX, 77550, USA

[4]Department of Pathology, University of Texas Medical Branch, Galveston, TX, 77555, USA

[5]Laboratory of Genetics and Helmsley Center for Genomic Medicine, The Salk Institute for Biological Sciences, La Jolla, CA 92037, USA

[6]Integral Molecular, Inc., Philadelphia, PA

[7]Department of Pathology, Microbiology and Immunology, Vanderbilt University Medical Center, Nashville, TN 37232, USA

[8]Department of Microbiology & Immunology, University of Texas Medical Branch, Galveston, TX, 77555, USA

[9]Department of Pediatrics, Vanderbilt University Medical Center, Nashville, TN 37232, USA

*Currently at NanoImaging Services Inc., San Diego, CA

**Currently at Division of Biology and Biological Engineering, California Institute of Technology, Pasadena, CA, 91125, USA

†Corresponding author

Summary

Antibodies that target the glycan cap epitope on ebolavirus glycoprotein (GP) are common in the adaptive response of survivors. A subset is known to be broadly neutralizing, but the details of their epitopes and basis for neutralization is not well-understood. Here we present cryo-electron microscopy (cryo-EM) structures of several glycan cap antibodies that variably synergize with GP base-binding antibodies. These structures describe a conserved site of vulnerability that anchors the mucin-like domains (MLD) to the glycan cap, which we name the MLD-anchor and cradle. Antibodies that bind to the MLD-cradle share common features, including the use of *IGHV1-69* and *IGHJ6* germline genes, which exploit hydrophobic residues and form beta-hairpin structures to mimic the MLD-anchor, disrupt MLD attachment, destabilize GP quaternary structure and block cleavage events required for receptor binding. Our results collectively provide a molecular basis for ebolavirus neutralization by broadly reactive glycan cap antibodies.

Keywords: ebolaviruses, Ebola virus, antibody therapeutics, filoviruses, glycan cap, antibody, mAbs, broadly neutralizing

Introduction

There is mounting evidence that protection from filoviral infection can be achieved through the use of monoclonal antibodies (mAbs) that target the GP surface (Bornholdt et al., 2019; Brannan et al., 2019; Mire et al., 2017; Qiu et al., 2014; Saphire et al., 2018b). Several structures of antigen-antibody complexes in recent years indicate that antibodies can access nearly any region on the surface of GP (Flyak et al., 2015; Flyak et al., 2018; Gilchuk et al., 2018; Milligan et al., 2019; Murin, 2018; Murin et al., 2019; Pallesen et al., 2016; Pascal et al., 2018; Saphire et al., 2018a; Wec et al., 2017; West et al., 2018; Zhao et al., 2017). Such antibodies have utility as post-exposure therapeutics when used in combination, such as the tri-mAb cocktail REGN-EB3, which demonstrated high efficacy in animal models (Pascal et al., 2018) and in a clinical trial carried out during a recent Ebola virus (EBOV) outbreak (Mulangu et al., 2019). REGN-EB3 is only effective against EBOV, however a pan-ebolavirus therapeutic that recognizes multiple ebolaviruses that cause severe disease in humans and major outbreaks, including Bundibugyo virus (BDBV) and Sudan virus (SUDV), would be ideal given the unpredictability of ebolavirus outbreaks.

Cross-reactive antibodies often target regions of conserved sequence vital to viral function, such as the receptor binding site (RBS) (Flyak et al., 2015; Hashiguchi et al., 2015; Howell et al., 2016; King et al., 2018), the internal fusion loop (IFL) (Milligan et al., 2019; Murin, 2018; West et al., 2018; Zhao et al., 2017), the base of GP (Gilchuk et al., 2018; Misasi et al., 2016) and the heptad repeat 2 (HR2) region (Bornholdt et al., 2016b; Flyak et al., 2018). Less conserved regions, such as the glycan cap and MLD, also can be targeted by protective antibodies and typically represent the largest antibody responses found in survivors; however, such antibodies are usually weakly or non-neutralizing and species-specific (Murin et al., 2014; Zeitlin et al., 2011). For example, the antibody 13C6, which was included in the antibody cocktail ZMapp™, targets the

glycan cap, but is low in potency for viral neutralization and is thought to instead provide protection by facilitating a superior cellular response (Murin et al., 2014; Pallesen et al., 2016). Furthermore, the glycan cap/head epitope in the trimeric membrane form of GP is also partially present on sGP, the soluble dimer of GP that is secreted in abundance during natural infection (Cook and Lee, 2013; de La Vega et al., 2015; Pallesen et al., 2016). Finally, GP is massively remodeled during endosomal entry in processes mediated by host proteases, during which the glycan cap and MLD are removed (Bornholdt et al., 2016a; Lee and Saphire, 2009). Nevertheless, several antibodies have been identified that bind within the glycan cap and potently neutralize EBOV, BDBV and SUDV (Bornholdt et al., 2016b; Flyak et al., 2016; Gilchuk et al., 2020; Misasi et al., 2016; Murin et al., 2014; Pascal et al., 2018; Saphire et al., 2018a). The mechanistic basis for this activity, however, is not well-explored.

We previously characterized pan-ebolavirus neutralizing mAbs isolated from a survivor cohort of the EBOV 2013-2016 outbreak (Gilchuk et al., 2018; Gilchuk et al., 2020). Several antibodies that recognize the glycan cap revealed synergistic activity for the GP binding and virus neutralization when paired with GP base-binding antibodies. One such pair, EBOV-548 and EBOV-520, provided superior protection in animal models when compared with treatment by a single antibody. Structural evaluation revealed that EBOV-520 recognized the 3_{10} pocket that is partially shielded by the β17- β18 loop in uncleaved GP. EBOV-548, which binds to the glycan cap, removed this steric hindrance by dislodging and mimicking the β18-β18′ hairpin obscuring the 3_{10} pocket. These data revealed a structural mechanism for synergy mediated by a glycan cap-directed antibody.

We sought to determine if glycan cap antibodies from other survivors also use similar mechanisms of protection and synergy as the EBOV-548/EBOV-520 combination (Bramble et al.,

2018; Flyak et al., 2015; Flyak et al., 2018; Flyak et al., 2016; Gilchuk et al., 2018). This collection of antibodies, including two mAbs from a newly described survivor cohort, were tested for their ability to enhance the activity of the GP base-region-binding broadly neutralizing antibodies EBOV-520 and EBOV-515 (Gilchuk et al., 2020). Additionally, we observed and quantified antibody-induced GP trimer instability. Subsequent analysis by cryo-EM revealed a conserved structural motif, similar to that found in EBOV-548, wherein a complementarity determining region (CDR) exhibited molecular mimicry of the β18-β18′ hairpin in GP. Finally, we also quantified the ability of glycan cap antibodies to block GP cleavage events necessary for receptor binding site exposure. Our data collectively provide evidence for a mechanism behind the activity of broadly neutralizing and synergistic glycan cap antibodies to ebolaviruses and suggest a rational strategy for the design of therapeutic antibody cocktails.

Results

Glycan cap antibody synergy is a common feature and is associated with GP instability

We previously described an assay to determine antibody binding synergy of pairs of antibodies for glycan cap antibody-based synergy of the base-region-binding antibodies EBOV-515 and EBOV-520 (Gilchuk et al., 2020). Here, we extended this assay to glycan cap antibodies from other survivor cohorts. We chose previously isolated antibodies based on similar properties to the synergistic glycan cap mAb EBOV-548, including: 1) synergy with EBOV-520 and/or EBOV-515, 2) broad reactivity and neutralization, 3) long CDRH3 loops, 4) cross-reactivity with sGP and/or 5) protection *in vivo*. Based on these criteria, we chose the following antibodies: BDBV-43, BDBV-329, BDBV-289, EBOV-442, EBOV-437 and EBOV-237 (Flyak et al., 2016; Gilchuk et al., 2018; Qiu et al., 2012; Williamson et al., 2019; Wilson et al., 2000). EBOV-548, 13C6, and an unrelated human mAb directed to dengue virus (DENV) envelope protein 2D22, were included for comparative purposes and as controls (**Table 1**). In addition, we also tested two new antibodies, EBOV-293 and EBOV-296, which we isolated from an individual treated for EBOV infection in the United States (**Table 1**, also see *Materials and Methods*). Ten characterized glycan cap antibodies potently bound to the sGP as judged by the half-maximal effective (EC_{50}) concentrations, and revealed diverse GP reactivity and virus neutralization profiles, and diverse protective efficacy in EBOV challenge mouse model (**Table 1, Fig. S1A**). In addition, epitope mapping by alanine scanning mutagenesis library analysis identified key contact residues for each antibody (**Table 1; Fig. S1B**). Furthermore, several of these antibodies have exceptionally long CDRH3 loops, such as the 33 amino acid loop of BDBV-329 (**Table S1**).

We then analyzed all ten glycan cap mAbs for binding enhancement of the base-region-directed mAbs EBOV-515 or EBOV-520 using an approach described previously (Gilchuk et al., 2020). Synergy for each glycan cap antibody followed similar patterns for EBOV-515 and EBOV-520, although enhancement of EBOV-520 binding appears higher likely due to differences in the molecular nature of the epitope (**Fig. 1A**). A steady range of synergistic patterns from no enhancement (for 13C6) to binding nearly equivalent to cleaved GP (GP_{CL}) (for EBOV-237) were observed (**Fig. 1A**). It should be noted that BDBV-329 and EBOV-237 are monospecific for the autologous virus BDBV or EBOV, respectively (**Table 1**).

We noticed in several of our 2D classes of glycan cap antibody complexes that the GP trimer fell apart into GP monomers, similar to what we had observed with our previous characterization of EBOV-548 (Gilchuk et al., 2020). The amount of GP trimer destabilization was variable across all the complexes, with some antibodies inducing a large amount of GP monomers and others only a stable GP trimer. We specifically avoid inclusion of monomers during protein purification to obtain a pure fraction of trimeric GP as starting material. We therefore hypothesized that glycan cap antibodies destabilize trimers, which in turn may contribute to their synergistic ability with base-region-binding antibodies.

To quantify GP destabilization, we analyzed cryo-EM data collected on glycan cap antibody complexes for structural analysis (*see below*). We also included previous data collected on EBOV-548 complexed with GP (Gilchuk et al., 2020). Particles were selected using a difference of gaussian approach which would not discriminate trimeric complexes from monomeric ones and then performed reference-free 2D classification (**Fig. 1B**). All trimeric and monomeric particles were subsequently subclassified and particle counts were used to determine the percentage of monomeric particles in the cleaned stack of total particles for each dataset.

When plotting the proportion of monomers formed in the presence of each glycan cap antibody, we noted that the amount of destabilization correlated with the extent of antibody synergy (**Fig. 1C**). Antibodies that did not synergize with base-region-binding antibodies displayed little to no destabilization, such as 13C6, BDBV-43, BDBV-329 and BDBV-289. As synergy increased, we saw increasing amounts of destabilized trimers, with EBOV-237 demonstrating the highest level of destabilization (**Fig. 1C**).

Conservation of a structural β-hairpin motif across synergistic glycan cap antibodies

To determine the structural basis of neutralization and synergy behind glycan cap antibody-based enhancement of base-region-binding antibodies, we solved eight structures of glycan cap antibodies in complex with mucin deleted (ΔMuc) EBOV GP (Makona) and BDBV GPΔMuc (**Fig. 2A-B, Fig. S2, Table S2**). Antibodies exhibited a range of angles-of-approach to GP, from obtuse, such as EBOV-437, to nearly parallel to the viral surface, like EBOV-237 (**Fig. 2C**). Additionally, the antibodies are spaced across the surface of GP inversely related to their angle-of-approach (**Fig. 2C**).

Resolutions achieved for glycan cap antibody cryo-EM structures ranged from 3.3 to 4.4 Å for six of our complexes (**Table S2, Fig. S2A-F**); however, preferred orientation, sub-stoichiometric Fab binding and trimer instability resulted in limited resolution for BDBV-329 and EBOV-237 bound structures (**Fig. S2G-H**). We did, however, model BDBV-329 where resolutions ranged from 4 to 5 Å at the antibody binding interface (**Fig. S2G**). The local resolutions for the EBOV-237 structure were particularly poor, and we therefore chose only to dock a homology model for interpretation (**Fig. S2H**). Most of our structures were determined in complex with EBOV-515 in order to assist with angular sampling and alignment, but we chose not to model

206 EBOV-515 and removed this density from our figures for clarity and to focus on glycan cap
207 antibodies (**Fig. 3A-B**).

208 All glycan cap antibodies make contacts exclusively within GP1 and are heavily biased
209 toward HC contacts (**Fig. 3, Table S3, Fig. S3**). Antibody contacts are focused on the β17 strand
210 of GP1 from residues 268-280 with a majority of contacts centered around W275 (**Fig. 3, Table**
211 **S3**), which when mutated to alanine abrogates binding (**Table 1, Fig. S1B**). Additionally, most
212 glycan cap antibodies make some contact with the inner head domain (**Fig. 3, Table S3, Fig. S3**).
213 These contacts are characterized by hydrogen bonding along the length of β17 with either short
214 CDRH2 loops for EBOV-293 (**Fig. 3A-B, Fig. S3A**) and BDBV-43 (**Fig. 3C-D, Fig. S3B**) or
215 extended, long (≥ 21 amino acids) CDRH3 loops for EBOV-437 (**Fig. 4F, Fig. S5C**), BDBV-289
216 (**Fig. 3G-H, Fig. S3D**), EBOV-442 (**Fig. 3I, Fig. S3E**) and EBOV-296 (**Fig. 3J-K, Fig. S3F**),
217 very similar to EBOV-548 as we previously reported (Gilchuk et al., 2020). Outside of the
218 hydrogen bonding that occurs along β17, several glycan cap antibodies make additional stabilizing
219 bonds, including hydrogen bonds, salt bridges, carbon-pi and pi-pi bonds with other portions of
220 GP1 (**Fig. 3**). Methionine-aromatic interactions also appear in several of the glycan cap antibodies,
221 particularly with W275 in GP1 (**Fig. 3D, H, J**). These types of interactions are thought to provide
222 additional stability compared to purely hydrophobic interactions, can act at long distances (~5-6
223 Å) and are thought to be less sensitive to changes in the local environment (Valley et al., 2012) ,
224 which may help contribute to increased breadth.

225 The CDRH3 loops of the glycan cap antibodies generally adopt an extended β-hairpin
226 motif with either partial or full β-strand secondary structure (**Fig. 4A**). These loops also pair with
227 β17 in GP1 to form an extended β-sheet and displace the β18-β18′ hairpin by mimicking its
228 structure, as was observed in our previous structure of EBOV-548 (**Fig. 4B**). BDBV-43 and

EBOV-293 alternatively use shorter CDRH2 loops to pair with β17 (**Fig. 4A-B**). Conversely, 13C6 has a much shorter CDRH3 loop and does not make full contact with β17 (**Fig. 4B**), possibly explaining its lack of synergy with base antibodies (**Fig. 1A**). EBOV-237 and BDBV-329 are unique among the antibodies we examined here owing to very long CDRH3 loops at 25 or 33 amino acids, respectively.

We also determined the unliganded crystal structure of BDBV-289 Fab to 3.0 Å resolution to compare the confirmations of the CDR loops prior to GP engagement (**Fig. 4C, Table S4**). The structure of the unliganded BDBV-289 Fab is very similar to BDBV-289 Fab bound to EBOV GPΔMuc, with an RMSD of 1.6 Å for the Fv portions of the HC and LC (**Fig. 4C**). There is a slight shift of the CDRL3 to accommodate the α2-β17 loop in the glycan cap, and a larger shift of CDRH3 (**Fig. 4C**). In the GP-bound structure, the CDRH3 loop moves toward GP by an average distance of ~3.3 Å (**Fig. 4C**). In the crystal structure, this movement is blocked by a crystal lattice interaction, but this difference may indicate flexibility in the tip of this loop.

The β18-β18′ hairpin anchors the mucin-like domains and shields a hydrophobic patch in the glycan cap

The β18-β18′ region of the glycan cap forms a β-hairpin that anchors the MLD, forming an extended beta sheet with the underlying core of GP1 (**Fig. 5A**) (Zhao et al., 2016). Due to the recurrence of the β18-β18′ hairpin epitope within the glycan cap and its role in anchoring down MLD, we have named this portion of the glycan cap the "MLD-anchor" (**Fig. 5A**). Upon binding of glycan cap antibody, the MLD-anchor is displaced, revealing a patch of hydrophobic residues, which we refer to as the "MLD-cradle" (**Fig. 5B**).

The MLD-anchor contains complementary hydrophobic residues along the β18′ strand that are buried by the MLD-cradle (**Fig. 5C**). Through molecular mimicry, the CDRH3 or CDRH2 loops of each of the neutralizing glycan cap antibodies characterized in this study bury analogous hydrophobic residues in the cradle, displacing the anchor (**Fig. 5C**). Our structures of EBOV-548 (Gilchuk et al., 2020) Fab and BDBV-289 Fab bound to GP indicate that although binding abrogates attachment of the MLD-anchor, the β17-β18 loop most likely remains tethered to the base of the IFL via $W291_{GP1}$ to $N512_{GP2}$. However, glycan cap binding may remove some restraint on the β17-β18 loop, allowing increased binding by GP base-directed antibodies.

The sequence of the N-terminal portion of the MLD-anchor (β18), the MLD-cradle and the β17-β18 loops are relatively conserved throughout all ebolaviruses, however, the surrounding regions in the glycan cap are not (**Fig. 5D-E, Fig. S4**). The glycan cap antibody contacts described here are focused toward β17 but other contacts outside this region are also observed (**Fig. S4, Table S3**). While each glycan cap antibody makes contacts outside the most conserved regions, there is less reliance on these regions for contact in the more cross-reactive antibodies (**Fig. S4**).

Germline analysis and conservation of features within glycan cap antibody paratopes

The glycan cap antibodies described here share several common features, including a majority (5 out of 9) deriving from the *IGHV1-69* germline gene segment (**Table S1**). Frequent use of the *IGHV1-69* gene is common in the antibody repertoires of those infected by influenza virus (Lang et al., 2017), HCV (Chan et al., 2001), HIV-1 (Huang et al., 2004), and other pathogens (Chen et al., 2019). The *IGHV1-69* gene is thought to be superior for viral neutralization at certain epitopes due to the presence of key germline encoded hydrophobic residues, especially in the CDRH2, as well as for breadth due to a large repertoire of allelic and copy number variations

(Chen et al., 2019). Despite a wide range of donors, we found these characteristics present in the ebolavirus antibodies described here (**Table S1, Fig. S5**).

Eight of the nine of the human antibodies described here use *IGHV1-69* and/or *IGHJ6* genes to form their HCs (**Table S1, Fig. S5**), the exception being EBOV-237. The use of *IGHV1-69* imparts a germline-encoded CDRH2 with several hydrophobic residues, which is used by BDBV-43 and EBOV-293 to bind to the MLD-cradle (**Fig. 5C**). In these cases, the CDRH3 loops are shorter (**Fig. S5**). For the rest of the glycan cap antibodies, usage of *IGHJ6* appears to be key, due to the presence of a patch of tyrosine residues in the germline gene which sit on the C-terminal end of the CDRH3 (**Fig. S5**). Overall, somatic hypermutation (SHM) was generally high throughout all glycan cap mAbs studied here, with an average of ~11% or ~6% amino change from germline for the V_H or V_L regions, respectively (**Table S1**).

Despite varying CDRH3 length, the tip of the CDRH3 hairpin contains a highly conserved glycine surrounded by hydrophobic residues and a C-terminal tyrosine motif (**Fig. 5F**). This glycine and hydrophobic tip help to insert the CDRH3 loop into the MLD-cradle (**Fig. 5A-C**) and assists in formation of the hairpin structure necessary for proper binding. The C-terminal tyrosine motif stabilizes longer CDRH3 loops within the core of the paratope and provides additional, non-specific hydrophobic contacts within the core of the epitope.

Glycan cap antibodies inhibit cleavage

The underlying molecular mechanism for how an antibody neutralizes is related to its ability to inhibit viral infection, which can be achieved by diverse mechanisms including cleavage inhibition. To determine the ability of the antibodies used in this study to inhibit cleavage, we performed a cleavage-blocking assay as previously described (Gilchuk et al., 2018) (**Fig. 6A**).

297 Jurkat cells stably transduced with EBOV GP (Jurkat-EBOV GP) were pre-incubated with
298 individual antibodies followed by treatment with thermolysin to mimic cathepsin cleavage to yield
299 membrane-displayed GP_{CL} (Jurkat-EBOV GP_{CL}). The exposure of the receptor binding site (RBS)
300 on GP_{CL} was measured by the level of binding of fluorescently labeled RBS-specific mAb MR78
301 that does not bind uncleaved EBOV GP (Flyak et al., 2015) The epitope of glycan cap antibodies
302 is being removed by cleavage, and in a separate assay we confirmed that none of tested antibodies,
303 except EBOV-442, compete with MR78 on Jurkat-EBOV GP_{CL} (**Fig. S6**). EBOV-442 partially
304 competed with MR78 (**Fig. S6**), suggesting incomplete removal of its epitope by thermolysin that
305 may have a minor effect on quantification of cleavage inhibition by this antibody. All EBOV GP-
306 reactive glycan cap antibodies revealed dose-dependent cleavage inhibition and most of them fully
307 blocked cleavage at the highest tested concentration of 60 μg/mL (**Fig. 6A**). Base antibody 2G4
308 and control antibody 2D22 did not inhibit cleavage. Although the glycan cap antibodies in this
309 study do not interact directly with the cathepsin cleavage loop, the disruption or dislocation of the
310 MLD may provide an obstacle for the recognition or cleavage activity by enzymes (**Fig. 6B**).
311
312
313
314
315
316
317
318
319

Discussion

Our previous structure of the EBOV-548/EBOV GP complex first revealed the glycan cap binding site containing the β18-β18′ hairpin (Gilchuk et al., 2020); however, the extensive structural evidence we provide here more completely describes this epitope, which we coin the MLD-anchor and cradle. The displacement of the MLD-anchor suggests that it is bound transiently, similar to the β17-β18 loop (West et al., 2019). Anecdotally, we and others have often noticed that the glycan cap is not well resolved in negative stain and cryo-EM structures of GP that lack coordinating glycan cap antibodies, suggesting this entire domain may be loosely attached to GP. This transient structural feature may aid in removal of the glycan cap upon cleavage for exposure of the NPC1 binding site. The MLD-anchor makes very limited contact with the underlying hydrophobic cradle, essentially mediated by a single β-strand. These characteristics have been observed for other antibodies that bind with hydrophobic, hairpin CDR loops, suggesting a conserved mechanism for neutralization that extends to other viruses (Lee et al., 2017; Pancera et al., 2010; Yuan et al., 2019).

Some of the antibodies in this study shared structural features that correlated with shared antibody germline gene usage, despite having been isolated from separate donors. For example, BDBV-43 and EBOV-293 are both encoded by the *IGHV1-69*09* gene allele, which is known to contain a germline-encoded hydrophobic CDRH2. These antibodies, accordingly, use their CDRH2 loops to access β17. However, several other antibodies in this study also use the *IGHV1-69* gene, but alternatively use longer CDRH3 loops to access β17. BDBV-43 and EBOV-293 also share almost identical LC usage (*IGKV3-15*01* and *3-20*01* for V_L genes and *IGKJ5*01* for J_L genes, respectively). Their structures are nearly identical as well, which indicates that LC pairing may influence access to β17 by *IGHV1-69* gene-encoded CDRH2 loops. However, this barrier can

be overcome through a larger number of non-templated (N) nucleotide additions within the CDRH3 when using alternative LC pairing. These observations may indicate that germline targeting vaccines could be an effective strategy for eliciting similar antibodies for EBOV in healthy individuals, similar to what has been shown in HIV-1 vaccine studies (Steichen et al., 2016; Steichen et al., 2019).

The glycan cap antibodies described here generally have high levels of SHM, with EBOV-293 containing 24 mutations from the inferred germline gene in its heavy chain (**Table S1**). This count also does not consider potential somatic mutations in the long CDRH3 loops, whose germline origins cannot be predicted but likely arise from large numbers of N-additions during the original V-D-J recombination event. How glycan cap antibody SHM compares to mutation frequency in antibodies directed toward other epitopes is not well explored, but the amount of SHM we observe for these neutralizing glycan cap mAbs is higher than is generally reported in EBOV survivor repertoires (Davis et al., 2019). Glycan cap antibodies are now known to form a large portion of the adaptive response to natural infection (Bornholdt et al., 2016b; Flyak et al., 2016; Wec et al., 2017). Several of these antibodies can potently neutralize, however, they are often mono-specific. It is unclear how the smaller subset of rarer, broadly neutralizing glycan cap antibodies develops. Our observations indicate that they may require higher levels of SHM combined with structural adaptations in order to reach cryptic epitopes shielded by the MLD, the MLD-anchor and glycans.

The mechanism of viral neutralization by glycan cap antibodies is unclear. Potentially, these antibodies could act indirectly by preventing access to a cleavage loop that is necessary to cleave during viral entry (Bornholdt et al., 2016a) (**Fig. 6B, part I**). The MLDs are large, accounting for over half of the mass of GP, unstructured and highly glycosylated. While the MLDs

on ebolaviruses are known to sit atop the GP, those on marburgviruses are thought to drape over the sides (Hashiguchi et al., 2015). This difference may occur because marburgviruses lack the structured glycan cap that is found in ebolaviruses (King et al., 2018). Consequently, the NPC1 receptor binding site is fully exposed on full-length GP in marburgviruses (Flyak et al., 2015), while it is hidden under the glycan cap and MLD on ebolaviruses. Therefore, the MLD-anchor appears to pin the MLD down to the top of ebolavirus GPs, keeping them above the GP and out of the way of the cleavage loop. Displacing the MLD-anchor may displace the MLDs themselves while retaining covalent attachment of these large domains to GP (**Fig. 6B, part II**). Within the dense environment of the ebolavirus surface, in which many GP spikes are known to crowd together in close proximity (Tran et al., 2014), this displacement may cause the MLD to drape over the cathepsin cleavage loops, thus blocking access by enzymes.

Overall, our data collectively provide the molecular basis for breadth of reactivity and virus neutralization by potent glycan cap antibodies and suggest a rational strategy for the design of broad therapeutic antibody cocktails.

Acknowledgements

This work was supported by NIH grants U19 AI109762 and U19 AI142785. T.A. is supported by a Kellogg Graduate Student Fellowship from Scripps Research. We would like to thank the Joint Center for Structural Genomics at Scripps Research and Henry Tien for assistance with setting up crystal trays. We like to thank Dr. Robyn Stanfield for assistance with looping and shipping crystals, for assistance with collecting X-ray diffraction data, reducing the data and phasing the crystal structure. We also thank Dr. Ian Wilson for generously sharing synchrotron time to collect X-ray diffraction data. Use of the Stanford Synchrotron Radiation Lightsource, SLAC National Accelerator Laboratory, is supported by the U.S. Department of Energy, Office of Science, Office of Basic Energy Sciences under Contract No. DE-AC02-76SF00515. The SSRL Structural Molecular Biology Program is supported by the DOE Office of Biological and Environmental Research, and by the National Institutes of Health, National Institute of General Medical Sciences (including P41GM103393). The contents of this publication are solely the responsibility of the authors and do not necessarily represent the official views of NIGMS or NIH.

The Jurkat-EBOV GP cell line was a kind gift form Carl Davis and Rafi Ahmed. We thank Hannah Turner, Bill Anderson, Jonathan Torres, Gabriel Ozorowski and Charles Bowman from Scripps Research for their assistance with cryo-EM sample prep, microscope operation, data collection and processing.

Author contributions

C.D.M. performed protein production for all cryo-EM and kinetic experiments, performed cryo-EM experiments and analysis, crystallized the BDBV289 Fab and performed kinetic experiments and analysis. C.D.M. collected the crystal data and phased the data. J.F.B. built and

validated the crystal structure. J.C. produced antibody Fab for the crystallography trials. P.G. performed synergy, cleavage assays and assembled information for Table 1. T.A. helped to perform GP stability assays and collect cryo-EM data. L.W. expressed and purified EBOV-237 and BDBV-329 Fab. P.A.I., K.H., N.K., X.S., A.I.F. and A.B. isolated and characterized EBOV-293 and EBOV-296. A.L.B., E.D. and B.J.D. performed alanine scanning and characterization of EBOV-293 and EBOV-296. C.D.M., P.G., A.B., J.E.C. and A.B.W. designed the experiments. C.D.M. wrote the manuscript.

Declaration of Interests

A.L.B., E.D., and B.J.D. are employees of Integral Molecular. B.J.D. is a shareholder of Integral Molecular. J.E.C. has served as a consultant for Sanofi and is on the Scientific Advisory Boards of CompuVax and Meissa Vaccines, is a recipient of previous unrelated research grants from Moderna and Sanofi and is founder of IDBiologics. Vanderbilt University has applied for a patent that is related to this work. All other authors declare no competing interests.

435 **Figure Legends**

436

437 **Figure 1. Glycan cap antibody synergy and GP destabilization. A)** Jurkat cell-surface
438 displayed EBOV GP binding was assessed using fluorescently labeled EBOV-515 or EBOV-520
439 after prior incubation of cells with individual unlabeled glycan cap antibodies. The blue dotted
440 line represents basal binding of base antibodies without glycan cap antibodies. The orange dotted
441 line represents maximal binding of base antibodies to cleaved GP. Data shown as mean ± SD of
442 technical triplicates **B)** Negative stain 2D-class averages of GP complexes bound to glycan cap
443 antibodies and EBOV-515 demonstrating examples of intact, trimeric complexes (left) and
444 monomeric complexes (right). **C)** Correlation analysis of antibody synergy and GP
445 destabilization by glycan cap antibodies.

446

447 **Figure 2. Neutralizing and synergistic glycan cap antibodies bind GP across a wide range**
448 **of orientations. A)** Low-pass filtered glycan cap Fabs from cryo-EM structures solved in this
449 study, as well as elsewhere, bound to EBOV GPΔMuc are overlaid to compare binding epitope
450 and angle-of-approach. **B)** Surface representations of cryo-EM structures solved in this study
451 with a fitted ribbon model protomer. Shown are side (left) or top (right) views with respect to the
452 viral membrane. Fab HC is colored in dark tones and LC in light tones. Co-binding antibodies
453 were removed from reconstructions for clarity. **C)** Relationship between antibody angle-of-
454 approach and Fab spacing. An angle-of-approach of zero degrees is considered parallel and 90°
455 is considered perpendicular to the viral surface. An angle-of-approach greater than 90° indicates
456 antibodies that bind inward toward the head domain while less than 0° indicates antibodies that
457 bind upward from the viral membrane. Fab spacing is determined by averaging the distance from

458 the same point on modeled Fab hinge terminal residues in the HC and LC. Antibodies are labeled
459 as in part A. See also Figure S2 and Figure S4.
460
461 **Figure 3. Structural details of glycan cap antibody binding to GP.** Single protomers from
462 structural models are shown with close-up views of interacting regions. HCs are rendered in
463 darker colors and LCs in lighter colors, with GP1 colored white. Important residues that
464 coordinate interaction and binding are highlighted. **A)** Key residues in the EBOV-293 CDRH2
465 hydrogen bond along the length of β17 with an additional potential salt bridge between $E65_{H2}$
466 and $K276_{GP1}$. **B)** The EBOV-293 CDRH2 and H3 make additional contacts, including at W275,
467 and the LC forms potential hydrogen bonds between α2 and β17. **C)** Similar to EBOV-293, the
468 BDBV-43 CDRH2 loop binds along β17. **D)** The BDBV-43 CDRH2 makes additional contacts
469 at W275 and also contacts the loop between α2 and β17 via its LC. **E)** The EBOV-43 CDRH3
470 loop displaces the loop between α2 and β17, shifting N268 by ~8 Å (apo-GP in white and
471 BDBV-43 bound GP in grey). **F)** EBOV-437 makes contact with GP exclusively with its HC,
472 hydrogen bonding along β17 with its CDRH3 and contacting the head domain in several places.
473 **G)** BDBV-289 makes extensive hydrogen bonds with its CDRH3 along β17. **H)** The BDBV-289
474 CDRH3 contacts W275 via methionine-aromatic and pi-pi interactions. Additional contacts are
475 made with the head domain of GP via hydrophobic interactions with the CDRH2. **I)** BDBV-442
476 makes contact with GP exclusively with its HC. The CDRH3 makes hydrogen bonds along β17,
477 with W275 with hydrophobic interactions and along the loop between α2 and β17. **J)** EBOV-296
478 binds to GP along β17, contacting W275 via methionine-aromatic and pi-pi interactions. The LC
479 makes further contact to the head domain of GP with several potential salt bridges. **K)** The

480 EBOV-296 LC also makes contact to the loop between α2 and β17. See also Figure S3 and
481 Figure S4, Table S2 and Table S3.
482
483 **Figure 4. Glycan cap antibody paratopes feature long CDRH3 or short CDRH2 loops with**
484 **beta-hairpin structures that mimic and displace the β18- β18′ region in the glycan cap. A)**
485 Ribbon models of the glycan cap antibody Fv domains with CDR loops highlighted. The HC is
486 in dark gray (right) and the LC is in light grey (left). **B)** Structures highlighting the interaction of
487 each of the glycan cap antibodies with the β17 strand, which forms the basis of an extended beta
488 sheet in the glycan cap with the β17- β18 loop and β18- β18′ hairpin motif (shown on the left).
489 **C)** Crystal structure of BDBV-289 Fab. Shown on the right is comparison of the apo- and GP-
490 bound forms of BDBV-289. *From a previous study; †shown as an initial homology model.
491 EBOV-548 (PDB 6UYE) and 13C6 (PDB 5KEL) are included in this figure for comparison. See
492 also Figure S5, Table S2 and Table S4.
493
494 **Figure 5. Glycan cap antibodies target a conserved, hydrophobic cradle that anchors the**
495 **mucin-like domains to GP1. A)** Hydrophobicity surface rendering of apo-EBOV GP protomer
496 (PDB 5JQ3) with the MLD-anchor (β18- β18′) highlighted in red. Using the Kyte and Doolittle
497 scale (Kyte and Doolittle, 1982), hydrophobic residues are colored orange with hydrophilic ones
498 in blue. **B)** Upon glycan cap mAb binding, the MLD-anchor is displaced, exposing a
499 hydrophobic pocket we term the "MLD-cradle". The cradle lies within a groove formed by α2
500 and β17, directly above the 3^{10} pocket. Key residues of the cradle are indicated. The MLD-cradle
501 is composed of residues from α2 and β17 as well as some additional residues that lie deeper in
502 the core of GP1, including I218, F248, F252, L253, L256, I260, G264, L273, I274, W275, V277

and L244. The cradle is segmented in the middle by W275, which may explain this residue's pivotal role in the binding of many glycan cap antibodies to GP. **C)** Interaction of glycan cap mAb HC loops with the MLD-cradle (from the rectangle in panel B). Key hydrophobic residues from antibody paratopes are indicated. **D)** Sequence alignment of the MLD-anchor and cradle epitope for the five main ebolaviruses (EBOV Q05320, BDBV B8XCN0, SUDV Q66814, TAFV Q66810 and RESTV Q66799) with topology indicated below. Residues highlighted in orange are key hydrophobic residues that form the cradle, those in green form the base of the β17- β18 loop that interact with the base of the fusion loop, and those in red are key residues from β18 that interact with the cradle in apo-GP. Those marked with a * are common escape mutants for this epitope. **E)** Glycan cap antibody footprints highlighted on the structure of apo-GP colored to reflect conservation, with dark purple indicating complete lack of conservation and white indicating complete conservation. **F)** Shown is a sequence alignment of the CDRH3 region from each of the glycan cap antibodies analyzed in this study, with darker pink indicating complete conservation and light pink indicating complete lack of conservation. The beta-turn-beta structure common to these paratopes is indicated above. Key sequences that are similar among these antibodies are boxed in black with "Y" stretches from *IGHJ6* gene usage underlined in purple. See also Figure S5.

Figure 6. Cleavage inhibition by glycan cap antibodies. A) Jurkat-EBOV GP was incubated with various concentrations of antibodies, treated with thermolysin, and then assayed using flow cytometry for exposure of the receptor binding site (RBS) as measured by binding of a fluorescently labeled MR78 antibody that recognizes the RBS. Determined IC_{50} and IC_{90} values (left) and dose-dependent inhibition curves (right) are shown. Dotted line indicates % RBS

526 exposure in the presence of 2D22 control. BDBV-329 was excluded because it does not bind to
527 EBOV GP, and BDBV-43 was not tested due to poor recombinant expression. **B)** Proposed
528 model of the GP inhibition by glycan cap antibodies: I. Enzyme cleavage of a loop draped over
529 the outside of GP (magenta) is thought to release the glycan cap and attached MLD. II. Glycan
530 cap antibodies that bind to the MLD-cradle displace the MLD-anchor and thus the MLDs
531 themselves, potentially shifting their position and sterically blocking access to the cleavage loop
532 by enzymes, especially on a GP-dense viral surface. See also Figure S6.
533
534
535
536
537
538
539
540
541
542
543
544
545
546
547
548

Antibody	GP binding by ELISA, EC_{50} (ng/mL)				Virus neutralization, IC_{50} (ng/mL)			Site on GP	GP mutations	IgG therapy in mice (EBOV), % survival	Antibody source
	EBOV GP	BDBV GP	SUDV GP	EBOV sGP*	EBOV	BDBV	SUDV				
EBOV-293	49	198	91	3	1,672	1,892	10,456	GC	T240A, W275A	100*	This study
EBOV-296	39	78	514	4	5,758	534	39,217	GC	W275A	20*	This study
BDBV-329	>	135	>	21 (BDBV sGP)	>	770	>	GC	ND	ND	Flyak *et al.* 2016
BDBV-289	29	20	103	1	602	32	>	GC	W275A, Y241A	80	Flyak *et al.* 2016
BDBV-43	22	29	21	18 (BDBV sGP)	7,248	139	318	GC	L273P	20	Flyak *et al.* 2016
EBOV-237	25	3,367	>	162	780	ND	ND	GC	I260R, N278A, P279A, S322G	80-90**	Williamson *et al.* 2019
EBOV-437	3	11	4	1	8,660***	>	>	GC	W275A	ND	Gilchuk *et al.* 2018
EBOV-442	1	3	6	1	467	1,489	<75%***	GC	W275A, L273P	80	Gilchuk *et al.* 2018
EBOV-548	6	7	132	1	1,601	2,262	<12%***	GC	T240A, R266A, T269A, T270A, I274A, W275	40	Gilchuk *et al.* 2020
13C6	20	>	>	2	>	>	>	GC	T270A, K272A, T240N	100	Wilson *et al.* 2000
2G4	203	>	>	>	139	>	>	Base	C511A, G553A, N550A, D552A, C556A, Q508R	60	Qiu *et al.* 2012

Table 1. Summary of binding and functional activities of characterized antibodies.

Characteristics for previously described antibodies were included for comparative purposes. *Determined in this study; ** prophylaxis efficacy; ***incomplete neutralization at highest tested Ab concentration (0.2 mg/mL); ">" indicates activity was not detected at highest tested Ab concentration; ND – not determined. See also Figure S1 and Table S1.

STAR Methods

RESOURCE AVAILABILITY

Lead contact

Further information regarding requests for resources and reagents should be directed to and will be fulfilled by the Lead Contact, Andrew Ward (andrew@scripps.edu).

Materials availability

Plasmids generated in this study are available upon request by the Lead Contact.

Data and code availability

The cryo-EM maps and structural coordinates generated during this study are available at the Electron Microscopy Data Bank (www.ebi.ac.uk/pdbe/emdb) and the Worldwide Protein Data Bank (www.pdb.org). The accession codes for the following cryo-EM maps reported in this paper are: EMD-22839 (EBOV GPΔMuc:BDBV289 Fab), EMD-22841 (BDBV GPΔMuc:BDBV43 Fab and ADI-15878 Fab), EMD-22853 (EBOV GPΔMuc:EBOV-437 Fab and EBOV-515 Fab), EMD-22848 (EBOV GPΔMuc:EBOV-442 Fab and EBOV-515 Fab), EMD-22842 (EBOV GPΔMuc:EBOV-293 Fab and EBOV-515 Fab), EMD-22847 (EBOV GPΔMuc:EBOV-296 Fab and EBOV-515 Fab), EMD-22851 (EBOV GPΔMuc:BDBV-329 Fab and EBOV-515 Fab) and EMD-22852 (EBOV GPΔMuc:EBOV-237 Fab and EBOV-515 Fab). The accession codes for PDB files are: 7KEJ (EBOV GPΔMuc:BDBV-289 Fab), 7KEW (BDBV GPΔMuc:BDBV-43 Fab), 7KFH (EBOV GPΔMuc:EBOV-437 Fab), 7KFB (EBOV GPΔMuc:EBOV-442 Fab), 7KEX

579 (EBOV GPΔMuc:EBOV-293 Fab), 7KF9 (EBOV GPΔMuc:EBOV-296 Fab), 7KFE (EBOV
580 GPΔMuc:BDBV-329 Fab) and 7KFG (unliganded BDBV289 Fab).
581
582 **EXPERIMENTAL MODEL AND SUBJECT DETAILS**
583 *Human samples*
584 Human PBMCs were obtained from a survivor of the 2014 EVD epidemic who acquired
585 the infection in the Democratic Republic of Congo and was treated in the Nebraska Medical Center
586 in the United States. A male human survivor was age 57 when PBMCs were collected. PBMCs
587 were collected after the illness had resolved, following written informed consent. The studies were
588 approved by the Institutional Review Board of Vanderbilt University Medical Center.
589
590 *Cell lines*
591 Suspension adapted HEK293F cells were obtained from ThermoFisher Scientific and
592 cultured in serum-free FreeStyle medium. Cells were maintained in shaking incubators at 100%
593 humidity, 37°C and 8% CO_2. Expi293F cells (ThermoFisher Scientific) were maintained at 37 °C
594 in 8% CO_2 in Expi293F Expression Medium (ThermoFisher Scientific). ExpiCHO cells
595 (ThermoFisher Scientific) were maintained at 37°C in 8% CO_2 in ExpiCHO Expression Medium
596 (ThermoFisher Scientific). The Jurkat-EBOV GP (variant Makona) cell line stably transduced to
597 display respective GP on the surface (Davis et al., 2019) was a kind gift from Carl Davis (Emory
598 University, Atlanta, GA). Jurkat-EBOV GP cells were maintained at 37°C in 8% CO_2 in RPMI-
599 1640 medium (Gibco) supplemented with 10% fetal heat-inactivated fetal bovine serum (FBS).
600 Mycoplasma testing of Expi293F and ExpiCHO cultures was performed on a monthly basis using

a PCR-based mycoplasma detection kit (ATCC). Cell lines were not authenticated following purchase.

Viruses

Mouse-adapted EBOV Mayinga (EBOV-MA, GenBank: AF49101) virus was described previously (Bray et al., 1998).

Mouse models

Seven- to eight-week old female BALB/c mice were obtained from the Jackson Laboratory. Mice were housed in microisolator cages and provided food and water *ad libitum*. Challenge studies were conducted under maximum containment in an animal biosafety level 4 (ABSL-4) facility of the Galveston National Laboratory, UTMB. The animal protocols for testing of mAbs in mice were approved by the Institutional Animal Care and Use Committee (IACUC) of the University of Texas Medical Branch in compliance with the Animal Welfare Act and other applicable federal statutes and regulations relating to animals and experiments involving animals.

METHOD DETAILS

Isolation of mAbs EBOV-293 and EBOV-296

Hybridoma cell lines secreting human mAbs were generated as described previously (Flyak et al., 2018). In brief, previously cryopreserved samples were transformed with Epstein-Barr virus, CpG and additional supplements. After 7 days, cells from each well of the 384-well culture plates were expanded into four 96-well culture plates using cell culture medium containing irradiated heterologous human PBMCs (recovered from blood unit leukofiltration

624 filters, Nashville Red Cross) and incubated for an additional four days. Plates were screened for
625 EBOV GP antigen-specific antibody-secreting cell lines using enzyme-linked immunosorbent
626 assays (ELISAs). Cells from wells with supernatants reacting with antigen in an ELISA were
627 fused with HMMA2.5 myeloma cells using an established electrofusion technique (Yu et al.,
628 2008). Antibody heavy- and light-chain variable region genes were sequenced from hybridoma
629 lines that had been cloned biologically by single-cell flow cytometric sorting. Briefly, total RNA
630 was extracted using the RNeasy Mini kit (QIAGEN) and reverse-transcriptase PCR (RT-PCR)
631 amplification of the antibody gene cDNAs was performed using the PrimeScript One Step RT-
632 PCR kit (CLONTECH) according to the manufacturer's protocols with gene-specific primers
633 (Thornburg et al., 2016). The thermal cycling conditions were as follows: 50°C for 30 min, 94°C
634 for 2 min, 40 cycles of (94°C for 30 s, 58°C for 30 s and 72°C for 1 min). PCR products were
635 purified using Agencourt AMPure XP magnetic beads (Beckman Coulter) and sequenced
636 directly using an ABI3700 automated DNA sequencer. The identities of gene segments and
637 mutations from germlines were determined by alignment using the ImMunoGeneTics database
638 (Giudicelli and Lefranc, 2011).
639
640 *Synergistic binding to cell-surface-displayed GP*
641 The assay was performed as described previously (Gilchuk et al., 2018). Briefly, Jurkat-
642 EBOV GP cells were pre-incubated at 4°C for 30 min with individual unlabeled glycan cap-
643 specific mAbs at a saturating for GP binding concentration (20 μg/mL) in PBS containing 2%
644 FBS and 2 mM EDTA, and then Alexa Fluor 647-labeled mAbs EBOV-515 or EBOV-520 were
645 added to a total concentration of labeled mAbs of 10 μg/mL. Cells were incubated at 4°C for
646 additional 2 h, then washed and antibody binding was analyzed by flow cytometry using an iQue

Screener Plus flow cytometer (Intellicyt). Controls included binding of labeled mAb to mock-transduced Jurkat cells (background), binding of labeled mAb alone to intact Jurkat-EBOV GP (a baseline level of binding to calculate fold change in a presence of glycan mAb), and binding of labeled mAb alone to cleaved Jurkat-EBOV-GP (maximal saturating binding signal). Results are expressed as fold-increase in median fluorescence intensity (MFI) of labeled mAb binding in the presence of the tested unlabeled mAb minus background signal from mock control.

ELISA binding assays

To assess mAb binding at different pH, wells of 96-well microtiter plates were coated with purified, recombinant EBOV, BDBV or SUDV GPΔTM ectodomains or EBOV sGP at 4˚C overnight. Plates were blocked with 2% non-fat dry milk and 2% normal goat serum in DPBS containing 0.05% Tween-20 (DPBS-T) for 1 h. Purified mAbs were diluted serially in DPBS-T (pH 7.4), or DPBS-T that was adjusted to pH 5.5 or 4.5 with hydrochloric acid, added to the wells and incubated for 1 h at ambient temperature. The bound antibodies were detected using goat anti-human IgG conjugated with horseradish peroxidase (Southern Biotech) diluted in blocking buffer and TMB substrate (ThermoFisher Scientific). Color development was monitored, 1N hydrochloric acid was added to stop the reaction, and the absorbance was measured at 450 nm using a spectrophotometer (Biotek).

Epitope mapping using an EBOV GP alanine-scan mutation library

Epitope mapping was carried out as described previously (Gilchuk et al., 2018). Comprehensive alanine scanning (‘shotgun mutagenesis’) was carried out on an expression construct for EBOV GP (Yambuku-Mayinga variant) lacking the mucin-like domain (residues

311-461), mutagenizing GP residues 33-310 and 462-676 to create a library of clones, each representing an individual point mutant. Residues were changed to alanine (with alanine residues changed to serine). The resulting library, covering 492 of 493 (99.9%) of target residues, was arrayed into 384-well plates, one mutant per well, then transfected into HEK-293T cells and allowed to express for 22 hrs. Cells, unfixed or fixed in 4% paraformaldehyde, were incubated with primary antibody and then with an Alexa Fluor 488-conjugated secondary antibody (Jackson ImmunoResearch Laboratories). After washing, cellular fluorescence was detected using the Intellicyt flow cytometer. MAb reactivity against each mutant EBOV GP clone was calculated relative to wild-type EBOV GP reactivity by subtracting the signal from mock-transfected controls and normalizing to the signal from wild-type GP-transfected controls. Mutated residues within clones were identified as critical to the mAb epitope if they did not support reactivity of the test mAb but did support reactivity of other control EBOV mAbs. This counter-screen strategy facilitated the exclusion of GP mutants that were misfolded locally or that exhibited an expression defect. The detailed algorithms used to interpret shotgun mutagenesis data were described previously (Davidson and Doranz, 2014).

Mouse challenge and protection studies

Groups of 7-8-week-old female BALB/c mice (n = 5 per group) housed in microisolator cages were inoculated with 1,000 PFU of the EBOV-MA by the intraperitoneal (i.p.) route. Mice were treated i.p. with 100 µg (~5 mg/kg) of individual mAb per mouse on 1 dpi. Human mAb 2D22 (specific to an unrelated target, dengue virus) served as a negative control (Fibriansah and Lok, 2016). Mice were monitored twice daily from day 0 to 14 post infection for illness, survival, and weight loss, followed by once daily monitoring from 15 dpi to the end of the study

693 at 28 dpi. The extent of disease was scored using the following parameters: dyspnea (possible
694 scores 0–5), recumbence (0–5), unresponsiveness (0–5), and bleeding/hemorrhage (0–5).
695 Moribund mice were euthanized as per the IACUC-approved protocol. All mice were euthanized
696 on day 28 after EBOV challenge.
697
698 *Cryo-EM trimer stability assay*
699 Complexes for trimer stability assays were derived from data collected for structural
700 evaluation (*see Cryo-EM sample preparation* section below). Particle picks were completed using
701 a difference of gaussian method with low thresholds in order to pick everything on the grids.
702 Particles were separated into stacks for either intact particles or particles that were falling apart,
703 which was judged by eye, and then counted to determine approximate percentage of glycan cap
704 antibody-induced instability. We have previously determined that base binding antibodies alone
705 do not induce trimer instability.
706
707 *Cell surface displayed GP mAb competition-binding*
708 Jurkat-EBOV GP_{CL} cells were pre-incubated with a saturating concentration (typically
709 20 μg/mL) of glycan cap mAbs at room temperature for 30 min, followed by addition of labeled
710 antibody MR78 (Flyak et al., 2015; Hashiguchi et al., 2015) at 5 μg/mL and incubated for an
711 additional 30 min. Antibody MR78 was labeled with Alexa Fluor 647 and added after the first
712 mAb and without washing of cells to minimize a dissociation of the first mAb from cell surface
713 GP during a prolonged incubation. Cells were washed, fixed with 4% paraformaldehyde, and cell
714 staining was analyzed using an iQue Screener Plus flow cytometer flow cytometer. Background
715 values were determined from binding of the second labeled mAbs to untransfected Jurkat.

716 Results are expressed as the percent of binding in the presence of glycan cap mAb relative to
717 MR78 alone (maximal binding) minus background. The antibodies were considered competing if
718 the presence of first antibody reduced the signal of the second antibody to less than 35% of its
719 maximal binding or non-competing if the signal was greater than 86%. A level of 36–85% was
720 considered partial competition. Thermolysin cleavage removes the epitope for most tested glycan
721 cap antibodies that showed very low binding to Jurkat-EBOV GP_{CL} (data not shown). This study
722 served as an additional control to confirm that cleavage inhibition measured as percent of RBS
723 exposure is not due to MR78 binding completion with residually bound glycan cap antibody on
724 Jurkat-EBOV GP_{CL}.
725
726 *Cell surface displayed GP cleavage inhibition*
727 Jurkat-EBOV GP cells were pre-incubated with serial dilutions of mAbs in PBS for
728 20 min at room temperature, then incubated with thermolysin (Promega) for 20 min at 37°C. The
729 reaction was stopped by addition of the incubation buffer containing DPBS, 2% heat inactivated
730 FBS and 2 mM EDTA (pH 8.0). Washed cells were incubated with 5 μg/mL of fluorescently
731 labeled RBS-specific mAb MR78 at 4°C for 60 min. Stained cells were washed, fixed, and
732 analyzed by flow cytometry using iQue Screener Plus flow cytometer. Cells were gated for the
733 viable population. Background staining was determined from binding of the labeled mAb MR78
734 to Jurkat-EBOV GP (uncleaved) cells. Results are expressed as the percent of RBS exposure in
735 the presence of tested mAb relative to labeled MR78 mAb-only control (maximal binding to
736 Jurkat-EBOV GP_{CL}) minus background. The GP base-directed antibody 2G4 (Qiu et al., 2011)
737 and 2D22 served as negative controls. BDBV-329 was excluded because it does not bind to
738 EBOV and BDBV-43 was excluded due to poor recombinant expression of the antibody.

739

740 *Construct design, expression and protein purification*

741 EBOV GP (Makona) (residues 32-644, GenBank AKG65268.1) with an N-terminal tissue
742 plasminogen activator (*Homo sapiens*) signal sequence was codon optimized for mammalian
743 protein expression, synthesized and subcloned into the pPPI4 expression vector (GenScript). A C-
744 terminal enterokinase (Ek) cut site (DDDDK) was introduced after residue 628 followed by a short
745 linker (AG) and two streptavidin tags (WSHPQFEK) separated by a GS-linker
746 (GGGSGGGSGGGS). Residues 310-460 were removed to produce EBOV GPΔMuc. BDBV GP
747 (residues 1-643, GenBank ALT19772.1) with the GP-associated signal peptide, an Ek cut site after
748 residue 643 followed by an AG-linker and the double streptavidin tag as described above was
749 codon optimized for mammalian protein expression, synthesized and subcloned into pPPI4.
750 Residues 313-470 were removed to produce BDBV GPΔMuc. EBOV sGP (Mayinga) (residues 1-
751 314, GenBank AAD14584.1) with the sGP-associated signal peptide an enterokinase cut site after
752 residue 314 followed by an AG-linker and a double streptavidin tag was codon optimized for
753 mammalian protein expression, synthesized and subcloned into pPPI4.

754 All GPs were expressed and purified in transiently transfected HEK-293F cells at a density
755 of 0.8-1.5 x 10^6 cells/mL using 750 μg of DNA and 2.25 mg of polyethylenimine "Max" (MW
756 25,000, Polyscience, Inc.) mixed with 50 mL of Opti-MEM (ThermoFisher Scientific). Solutions
757 were sterile filtered using 0.22 μm Steriflip disposable filters (Millipore) and allowed to incubate
758 at room temperature for 30 min before being added to cultures. After 5 days of expression at 37°C
759 and 8% CO_2, cells were harvested by centrifugation (8,000 x g for 1hr at 4°C) and filtered to
760 remove cellular debris. BioLock biotin blocking solution (IBA Lifesciences) was added to
761 supernatant according to the manufacturer's protocol before being loaded onto Strep-Tactin

762 Superflow Plus beads (Qiagen) that had been pre-equilibrated in 1X Strep Buffer (100 mM Tris,
763 pH 8.0, 150 mM NaCl and 1mM EDTA). Beads were washed with 10 mL of 1X Strep Buffer and
764 GPs were eluted by addition of 2.5 mM d-desthiobiotin added to 10 mL of 1X Strep Buffer. GPs
765 were further purified by size exclusion chromatography (SEC) using an S200 increase (S200I, GE)
766 column equilibrated in 1X TBS (150 mM NaCl, 20 mM Tris, pH 7.4).

767 For EBOV-237, BDBV-329, EBOV-442, EBOV-437 and 2D22 recombinant mAb
768 production, cDNA encoding the genes of heavy and light chains were cloned into the pTwist CMV
769 Betaglobin WPRE Neo vector encoding IgG1 or Fab- heavy chain (McLean et al., 2000), or
770 monocistronic expression vector pTwist-mCis_G1 (Zost et al., 2020) and transformed into E. coli
771 cells. mAb proteins were produced after transient transfection of ExpiCHO cells following the
772 manufacturer's protocol and were purified from filtered culture supernatants by fast protein liquid
773 chromatography (FPLC) on an AKTA instrument using HiTrap MabSelect Sure column for IgG
774 (GE Healthcare Life Sciences) or CaptureSelect™ IgG-CH1 column for Fab (ThermoFisher
775 Scientific). Purified mAbs were buffer exchanged into PBS, filtered using sterile 0.45 μm pore
776 size filter devices (Millipore), concentrated, and stored in aliquots at −80°C until use.

777 For BDBV-289, BDBV-43, EBOV-293 and EBOV-296 antibody expression, sequences
778 were optimized for mammalian expression, synthesized and subcloned into the expression vector
779 AbVec containing the human IgG HC constant region or the human lambda or kappa LC constant
780 region (GenScript). Fab was produced by the introduction of a stop codon after residue 226 in the
781 HC hinge-region. ADI-15878 Fab and ADI-16061 Fab were used as a fiducials in this study and
782 were produced as previously described (Murin et al., 2018). IgGs and Fab were transiently
783 transfected as described above for GPs, except that 500 μg of HC DNA and 250 μg of LC DNA
784 was mixed to encourage HC/LC pairing and the avoidance of LC dimers. For BDBV-289 and

BDBV-43 Fab, cell supernatants were loaded onto 5 mL Lambda (BDBV-289) or Kappa (BDBV-43) Select columns (GE) that had been equilibrated in 1X phosphate buffered saline (PBS, QualityBiological) followed by elution with 0.1 M glycine, pH 3.0. Fab were subsequently buffer exchanged into 20 mM sodium acetate (NaOAc), pH 5.6 by dialysis and loaded onto a MonoS column (GE). Fab were then eluted with a gradient of 1M KCl. For EBOV-437, EBOV-442, EBOV-293 and EBOV-296 Fab, cell supernatants were loaded onto a 1 mL or 5 mL Capture Select column (ThermoFisher Scientific) and eluted with 0.1 M glycine, pH 3.0. Appropriate fractions were pooled and further purified by SEC using an S200I column equilibrated in 1X TBS buffer. For IgG, supernatants were loaded onto a HiTrap 5 mL mAb Select column (GE) that had been pre-equilibrated in 1X PBS followed by elution with 0.1 M glycine, pH 3.0 and neutralization with 1M Tris, pH 8.5. Appropriate fractions were pooled and further purified by SEC using an S200I column that had been equilibrated with 1X TBS.

Crystallization and Structure Determination of BDBV-289 Fab

Fabs produced for crystallographic studies were made in Expi-CHO cells per the manufacturer's "max titer" protocol (GIBCO/ThermoFisher Scientific) and purified as described above. BDBV-289 Fab was screened for crystallization using the Joint Center for Structural Genomics (JCSG) Rigaku CrystalMation at The Scripps Research Institute against the JCSG Core Suites I-IV. Protein at 7.4 mg/mL was mixed 1:1 with precipitants and crystallized using the vapor diffusion method at both room temperature and 4°C. Crystals grew in 0.1M HEPES pH 6.5 and 20% (w/v) polyethylene glycol 6000 at 4°C. Crystals were cryoprotected with well solution augmented with 30% ethylene glycol. Data were collected at Stanford Synchrotron Radiation Light Source beamline 12-2. Data were indexed, integrated and scaled using HKL-

2000 (Otwinowski and Minor, 1997) to 3.0 Å (Table S2). Crystals belonged to the space group $P6_1$ with a single Fab in the asymmetric unit.

Data were phased using Phaser (McCoy et al., 2007) with molecular replacement by a homology model generated using Swiss Modeler (Biasini et al., 2014). A single Fab was placed in the asymmetric unit. This initial solution was rebuilt manually in Coot (Emsley et al., 2010), followed by multiple rounds of refinement in Phenex.refine (Adams et al., 2010) and model building with Coot. Translation/Libration/Screw (TLS) groups were introduced towards the end of refinement. Four TLS groups were set manually with one for each immunoglobulin domain. A large positive density seen in the difference map was modeled as PEG after evaluating fits for all components of the buffer.

Cryo-EM sample preparation

EBOV/Mak GPΔmuc was incubated overnight with a 5-fold molar excess of each Fab at 4°C. The complexes were then purified by SEC using an S200I column equilibrated in 1X TBS and concentrated using a 100-kDa concentrator (Amicon Ultra, Millipore) and mixed with detergent immediately prior to freezing (**Table S2**). Vitrification was performed with a Vitrobot (ThermoFisher Scientific) equilibrated to 4°C and 100% humidity. Cryo-EM grids were plasma cleaned for 5s using a mixture of Ar/O_2 (Gatan Solarus 950 Plasma system) followed by blotting on both sides of the grid with filter paper (Whatman No. 1). See Table S1 for additional details for individual complexes. Note that ADI-15878 Fab was added to the BDBV-43 complex and ADI-16061 Fab and EBOV-515 Fab was added to the EBOV-437, EBOV-442, EBOV-293, EBOV-296, EBOV-237 and BDBV-329 complexes to assist in angular sampling and orientations in ice.

Cryo-EM data collection and processing

Cryo-EM data were collected according to Table S1. Micrographs were aligned and dose-weighted using MotionCor2 (Zheng et al., 2017). CTF estimation was completed using GCTF (Zhang, 2016). Particle picking and initial 2D classification were initially performed using CryoSPARC 2.0 (Punjani et al., 2017) to clean up particle stacks and exclude any complexes that were degrading. For those reconstructions that required more extensive 3D classification, particle picks were then imported into Relion 3.1b1 (Zivanov et al., 2018) for 3D classification and then refinement using appropriate symmetry where necessary and a tight mask around the GP/Fab complex of interest. CTF refinement was then performed by either Relion or CryoSPARC to increase map quality and resolution. There was no density for ADI-16061 in any of the maps and we did not build density for ADI-15878 in the BDBV-43 map (this was previously deposited under PDB 6DZM). We chose not to build a model into EBOV-515 density but included this density in our reconstructions to assist with particle alignment.

Cryo-EM model building and refinement

Homology models of Fab were first generated using SWISS-MODEL (Biasini et al., 2014). Models of BDBV GP (PDB: 6DZM) and EBOV GP (PDB: 5JQ3) were then added to generate starting models used for refinement. Models were fit into maps using UCSF Chimera (Pettersen et al., 2004) and refined initially using Phenix real-space refinement using NCS constraints (Liebschner et al., 2019). The refined model was then used as a template for relaxed refinement in Rosetta (DiMaio et al., 2015). The top five models were then evaluated for fit in EM density and adjusted manually using Coot (Emsley et al., 2010) to maximize fit. Finally, Man9 glycans were fit into glycan densities, trimmed and then a final refinement was performed in Rosetta. The final

854 structures were evaluated using EMRinger (Barad et al., 2015) and Molprobity from Phenix. All
855 figures were generated in UCSF Chimera (Pettersen et al., 2004). Antibody contacts were analyzed
856 using LigPlot (Laskowski and Swindells, 2011), Arpeggio (Jubb et al., 2017) and UCSF Chimera
857 (Pettersen et al., 2004).
858
859 *Inferred germline antibody analysis*
860 Inferred germline sequences for BDBV289 and BDBV43 F_V domains were determined
861 using IMGT/V-QUEST (Brochet et al., 2008; Giudicelli et al., 2011). Nucleotide sequences of B-
862 cells originally isolated from donors were kindly provided by James Crowe and used to derive a
863 list of likely germline VDJ genes. Those with the highest confidence were then used to reconstruct
864 an inferred germline sequence. The mature CDRH3 sequence was included in the reconstructed
865 germline sequences due to low confidence in predicting germline CDRH3 sequences, although
866 some residues were predicted to be different from the germline CDRH3. For BDBV-289 and
867 BDBV-43, inferred germline sequences were then codon optimized for mammalian protein
868 expression and sub-cloned into the appropriate AbVec expression vector. Stop codons were
869 introduced as described above to produce Fab.
870
871 **QUANTIFICATION AND STATISTICAL ANALYSIS**
872 The descriptive statistics mean ± SEM or mean ± SD were determined for continuous
873 variables as noted. EC_{50} values for mAb binding were determined after log transformation of
874 antibody concentration using sigmoidal dose-response nonlinear regression analysis. Correlation
875 between antibody synergy and percent monomer in GP trimer fraction was estimated using linear
876 regression analysis. In neutralization assays, IC_{50} values were calculated after log transformation

of antibody concentrations using a 4-parameter nonlinear fit analysis. Technical and biological replicates are indicated in the figure legends. Statistical analyses were performed using Prism v8 (GraphPad).

References

Adams, P.D., Afonine, P.V., Bunkoczi, G., Chen, V.B., Davis, I.W., Echols, N., Headd, J.J., Hung, L.W., Kapral, G.J., Grosse-Kunstleve, R.W., *et al.* (2010). PHENIX: a comprehensive Python-based system for macromolecular structure solution. Acta Crystallogr D Biol Crystallogr *66*, 213-221.

Barad, B.A., Echols, N., Wang, R.Y., Cheng, Y., DiMaio, F., Adams, P.D., and Fraser, J.S. (2015). EMRinger: side chain-directed model and map validation for 3D cryo-electron microscopy. Nat Methods *12*, 943-946.

Biasini, M., Bienert, S., Waterhouse, A., Arnold, K., Studer, G., Schmidt, T., Kiefer, F., Gallo Cassarino, T., Bertoni, M., Bordoli, L., *et al.* (2014). SWISS-MODEL: modelling protein tertiary and quaternary structure using evolutionary information. Nucleic Acids Res *42*, W252-258.

Bornholdt, Z.A., Herbert, A.S., Mire, C.E., He, S., Cross, R.W., Wec, A.Z., Abelson, D.M., Geisbert, J.B., James, R.M., Rahim, M.N., *et al.* (2019). A Two-Antibody Pan-Ebolavirus Cocktail Confers Broad Therapeutic Protection in Ferrets and Nonhuman Primates. Cell Host Microbe *25*, 49-58 e45.

Bornholdt, Z.A., Ndungo, E., Fusco, M.L., Bale, S., Flyak, A.I., Crowe, J.E., Jr., Chandran, K., and Saphire, E.O. (2016a). Host-Primed Ebola Virus GP Exposes a Hydrophobic NPC1 Receptor-Binding Pocket, Revealing a Target for Broadly Neutralizing Antibodies. MBio *7*, e02154-02115.

920 Bornholdt, Z.A., Turner, H.L., Murin, C.D., Li, W., Sok, D., Souders, C.A., Piper, A.E., Goff,
921 A., Shamblin, J.D., Wollen, S.E.*, et al.* (2016b). Isolation of potent neutralizing antibodies from
922 a survivor of the 2014 Ebola virus outbreak. Science *351*, 1078-1083.

923 Bramble, M.S., Hoff, N., Gilchuk, P., Mukadi, P., Lu, K., Doshi, R.H., Steffen, I., Nicholson,
924 B.P., Lipson, A., Vashist, N.*, et al.* (2018). Pan-Filovirus Serum Neutralizing Antibodies in a
925 Subset of Congolese Ebolavirus Infection Survivors. J Infect Dis *218*, 1929-1936.

926 Brannan, J.M., He, S., Howell, K.A., Prugar, L.I., Zhu, W., Vu, H., Shulenin, S., Kailasan, S.,
927 Raina, H., Wong, G.*, et al.* (2019). Post-exposure immunotherapy for two ebolaviruses and
928 Marburg virus in nonhuman primates. Nat Commun *10*, 105.

929 Bray, M., Davis, K., Geisbert, T., Schmaljohn, C., and Huggins, J. (1998). A mouse model for
930 evaluation of prophylaxis and therapy of Ebola hemorrhagic fever. J Infect Dis *178*, 651-661.

931 Brochet, X., Lefranc, M.P., and Giudicelli, V. (2008). IMGT/V-QUEST: the highly customized
932 and integrated system for IG and TR standardized V-J and V-D-J sequence analysis. Nucleic
933 Acids Res *36*, W503-508.

934 Chan, C.H., Hadlock, K.G., Foung, S.K., and Levy, S. (2001). V(H)1-69 gene is preferentially
935 used by hepatitis C virus-associated B cell lymphomas and by normal B cells responding to the
936 E2 viral antigen. Blood *97*, 1023-1026.

937 Chen, F., Tzarum, N., Wilson, I.A., and Law, M. (2019). VH1-69 antiviral broadly neutralizing
938 antibodies: genetics, structures, and relevance to rational vaccine design. Curr Opin Virol *34*,
939 149-159.

940 Cook, J.D., and Lee, J.E. (2013). The secret life of viral entry glycoproteins: moonlighting in
941 immune evasion. PLoS Pathog *9*, e1003258.

942 Davis, C.W., Jackson, K.J.L., McElroy, A.K., Halfmann, P., Huang, J., Chennareddy, C., Piper,
943 A.E., Leung, Y., Albarino, C.G., Crozier, I.*, et al.* (2019). Longitudinal Analysis of the Human B
944 Cell Response to Ebola Virus Infection. Cell *177*, 1566-1582 e1517.

945 de La Vega, M.A., Wong, G., Kobinger, G.P., and Qiu, X. (2015). The multiple roles of sGP in
946 Ebola pathogenesis. Viral Immunol *28*, 3-9.

947 DiMaio, F., Song, Y., Li, X., Brunner, M.J., Xu, C., Conticello, V., Egelman, E., Marlovits, T.,
948 Cheng, Y., and Baker, D. (2015). Atomic-accuracy models from 4.5-A cryo-electron microscopy
949 data with density-guided iterative local refinement. Nat Methods *12*, 361-365.

950 Emsley, P., Lohkamp, B., Scott, W.G., and Cowtan, K. (2010). Features and development of
951 Coot. Acta Crystallogr D Biol Crystallogr *66*, 486-501.

952 Fibriansah, G., and Lok, S.M. (2016). The development of therapeutic antibodies against dengue
953 virus. Antiviral Res *128*, 7-19.

954 Flyak, A.I., Ilinykh, P.A., Murin, C.D., Garron, T., Shen, X., Fusco, M.L., Hashiguchi, T.,
955 Bornholdt, Z.A., Slaughter, J.C., Sapparapu, G.*, et al.* (2015). Mechanism of human antibody-
956 mediated neutralization of Marburg virus. Cell *160*, 893-903.

957 Flyak, A.I., Kuzmina, N., Murin, C.D., Bryan, C., Davidson, E., Gilchuk, P., Gulka, C.P.,
958 Ilinykh, P.A., Shen, X., Huang, K.*, et al.* (2018). Broadly neutralizing antibodies from human

959 survivors target a conserved site in the Ebola virus glycoprotein HR2-MPER region. Nat
960 Microbiol *3*, 670-677.

961 Flyak, A.I., Shen, X., Murin, C.D., Turner, H.L., David, J.A., Fusco, M.L., Lampley, R., Kose,
962 N., Ilinykh, P.A., Kuzmina, N.*, et al.* (2016). Cross-Reactive and Potent Neutralizing Antibody
963 Responses in Human Survivors of Natural Ebolavirus Infection. Cell *164*, 392-405.

964 Gilchuk, P., Kuzmina, N., Ilinykh, P.A., Huang, K., Gunn, B.M., Bryan, A., Davidson, E.,
965 Doranz, B.J., Turner, H.L., Fusco, M.L.*, et al.* (2018). Multifunctional Pan-ebolavirus Antibody
966 Recognizes a Site of Broad Vulnerability on the Ebolavirus Glycoprotein. Immunity *49*, 363-374
967 e310.

968 Gilchuk, P., Murin, C.D., Milligan, J.C., Cross, R.W., Mire, C.E., Ilinykh, P.A., Huang, K.,
969 Kuzmina, N., Altman, P.X., Hui, S.*, et al.* (2020). Analysis of a Therapeutic Antibody Cocktail
970 Reveals Determinants for Cooperative and Broad Ebolavirus Neutralization. Immunity *52*, 388-
971 403 e312.

972 Giudicelli, V., Brochet, X., and Lefranc, M.P. (2011). IMGT/V-QUEST: IMGT standardized
973 analysis of the immunoglobulin (IG) and T cell receptor (TR) nucleotide sequences. Cold Spring
974 Harb Protoc *2011*, 695-715.

975 Giudicelli, V., and Lefranc, M.P. (2011). IMGT/junctionanalysis: IMGT standardized analysis of
976 the V-J and V-D-J junctions of the rearranged immunoglobulins (IG) and T cell receptors (TR).
977 Cold Spring Harb Protoc *2011*, 716-725.

978 Hashiguchi, T., Fusco, M.L., Bornholdt, Z.A., Lee, J.E., Flyak, A.I., Matsuoka, R., Kohda, D.,
979 Yanagi, Y., Hammel, M., Crowe, J.E., Jr., *et al.* (2015). Structural basis for Marburg virus
980 neutralization by a cross-reactive human antibody. Cell *160*, 904-912.

981 Howell, K.A., Qiu, X., Brannan, J.M., Bryan, C., Davidson, E., Holtsberg, F.W., Wec, A.Z.,
982 Shulenin, S., Biggins, J.E., Douglas, R., *et al.* (2016). Antibody Treatment of Ebola and Sudan
983 Virus Infection via a Uniquely Exposed Epitope within the Glycoprotein Receptor-Binding Site.
984 Cell Rep *15*, 1514-1526.

985 Huang, C.C., Venturi, M., Majeed, S., Moore, M.J., Phogat, S., Zhang, M.Y., Dimitrov, D.S.,
986 Hendrickson, W.A., Robinson, J., Sodroski, J., *et al.* (2004). Structural basis of tyrosine sulfation
987 and VH-gene usage in antibodies that recognize the HIV type 1 coreceptor-binding site on
988 gp120. Proc Natl Acad Sci U S A *101*, 2706-2711.

989 Jubb, H.C., Higueruelo, A.P., Ochoa-Montano, B., Pitt, W.R., Ascher, D.B., and Blundell, T.L.
990 (2017). Arpeggio: A Web Server for Calculating and Visualising Interatomic Interactions in
991 Protein Structures. J Mol Biol *429*, 365-371.

992 King, L.B., Fusco, M.L., Flyak, A.I., Ilinykh, P.A., Huang, K., Gunn, B., Kirchdoerfer, R.N.,
993 Hastie, K.M., Sangha, A.K., Meiler, J., *et al.* (2018). The Marburgvirus-Neutralizing Human
994 Monoclonal Antibody MR191 Targets a Conserved Site to Block Virus Receptor Binding. Cell
995 Host Microbe *23*, 101-109 e104.

996 Kyte, J., and Doolittle, R.F. (1982). A simple method for displaying the hydropathic character of
997 a protein. J Mol Biol *157*, 105-132.

998 Lang, S., Xie, J., Zhu, X., Wu, N.C., Lerner, R.A., and Wilson, I.A. (2017). Antibody 27F3
999 Broadly Targets Influenza A Group 1 and 2 Hemagglutinins through a Further Variation in VH1-
1000 69 Antibody Orientation on the HA Stem. Cell Rep *20*, 2935-2943.

1001 Laskowski, R.A., and Swindells, M.B. (2011). LigPlot+: multiple ligand-protein interaction
1002 diagrams for drug discovery. J Chem Inf Model *51*, 2778-2786.

1003 Lee, J.E., and Saphire, E.O. (2009). Ebolavirus glycoprotein structure and mechanism of entry.
1004 Future Virol *4*, 621-635.

1005 Lee, J.H., Andrabi, R., Su, C.Y., Yasmeen, A., Julien, J.P., Kong, L., Wu, N.C., McBride, R.,
1006 Sok, D., Pauthner, M.*, et al.* (2017). A Broadly Neutralizing Antibody Targets the Dynamic HIV
1007 Envelope Trimer Apex via a Long, Rigidified, and Anionic beta-Hairpin Structure. Immunity *46*,
1008 690-702.

1009 Liebschner, D., Afonine, P.V., Baker, M.L., Bunkoczi, G., Chen, V.B., Croll, T.I., Hintze, B.,
1010 Hung, L.W., Jain, S., McCoy, A.J.*, et al.* (2019). Macromolecular structure determination using
1011 X-rays, neutrons and electrons: recent developments in Phenix. Acta Crystallogr D Struct Biol
1012 *75*, 861-877.

1013 McCoy, A.J., Grosse-Kunstleve, R.W., Adams, P.D., Winn, M.D., Storoni, L.C., and Read, R.J.
1014 (2007). Phaser crystallographic software. J Appl Crystallogr *40*, 658-674.

1015 McLean, G.R., Nakouzi, A., Casadevall, A., and Green, N.S. (2000). Human and murine
1016 immunoglobulin expression vector cassettes. Mol Immunol *37*, 837-845.

1017 Milligan, J.C., Parekh, D.V., Fuller, K.M., Igarashi, M., Takada, A., and Saphire, E.O. (2019).
1018 Structural Characterization of Pan-Ebolavirus Antibody 6D6 Targeting the Fusion Peptide of the
1019 Surface Glycoprotein. J Infect Dis *219*, 415-419.

1020 Mire, C.E., Geisbert, J.B., Borisevich, V., Fenton, K.A., Agans, K.N., Flyak, A.I., Deer, D.J.,
1021 Steinkellner, H., Bohorov, O., Bohorova, N.*, et al.* (2017). Therapeutic treatment of Marburg and
1022 Ravn virus infection in nonhuman primates with a human monoclonal antibody. Sci Transl Med
1023 *9*.

1024 Misasi, J., Gilman, M.S., Kanekiyo, M., Gui, M., Cagigi, A., Mulangu, S., Corti, D.,
1025 Ledgerwood, J.E., Lanzavecchia, A., Cunningham, J.*, et al.* (2016). Structural and molecular
1026 basis for Ebola virus neutralization by protective human antibodies. Science *351*, 1343-1346.

1027 Mulangu, S., Dodd, L.E., Davey, R.T., Jr., Tshiani Mbaya, O., Proschan, M., Mukadi, D.,
1028 Lusakibanza Manzo, M., Nzolo, D., Tshomba Oloma, A., Ibanda, A.*, et al.* (2019). A
1029 Randomized, Controlled Trial of Ebola Virus Disease Therapeutics. N Engl J Med *381*, 2293-
1030 2303.

1031 Murin, C.D., Bruhn, J.F., Bornholdt, Z.A., Copps, J., Stanfield, R., and Ward, A.B. (2018).
1032 Structural Basis of Pan-Ebolavirus Neutralization by an Antibody Targeting the Glycoprotein
1033 Fusion Loop. Cell Rep *24*, 2723-2732 e2724.

1034 Murin, C.D., Bruhn, J. F., Bornholdt, Z. A., Copps, J., Stanfield, R., Ward, A. B. (2018).
1035 Structural basis of pan-ebolavirus neutralization by an antibody targeting the glycoprotein fusion
1036 loop. Cell Rep *24*, 2723-2732.

1037 Murin, C.D., Fusco, M.L., Bornholdt, Z.A., Qiu, X., Olinger, G.G., Zeitlin, L., Kobinger, G.P.,
1038 Ward, A.B., and Saphire, E.O. (2014). Structures of protective antibodies reveal sites of
1039 vulnerability on Ebola virus. Proc Natl Acad Sci U S A *111*, 17182-17187.

1040 Murin, C.D., Wilson, I.A., and Ward, A.B. (2019). Antibody responses to viral infections: a
1041 structural perspective across three different enveloped viruses. Nat Microbiol.

1042 Otwinowski, Z., and Minor, W. (1997). Processing of X-ray diffraction data collected in
1043 oscillation mode. Methods Enzymol *276*, 307-326.

1044 Pallesen, J., Murin, C.D., de Val, N., Cottrell, C.A., Hastie, K.M., Turner, H.L., Fusco, M.L.,
1045 Flyak, A.I., Zeitlin, L., Crowe, J.E., Jr.*, et al.* (2016). Structures of Ebola virus GP and sGP in
1046 complex with therapeutic antibodies. Nat Microbiol *1*, 16128.

1047 Pancera, M., McLellan, J.S., Wu, X., Zhu, J., Changela, A., Schmidt, S.D., Yang, Y., Zhou, T.,
1048 Phogat, S., Mascola, J.R.*, et al.* (2010). Crystal structure of PG16 and chimeric dissection with
1049 somatically related PG9: structure-function analysis of two quaternary-specific antibodies that
1050 effectively neutralize HIV-1. J Virol *84*, 8098-8110.

1051 Pascal, K.E., Dudgeon, D., Trefry, J.C., Anantpadma, M., Sakurai, Y., Murin, C.D., Turner,
1052 H.L., Fairhurst, J., Torres, M., Rafique, A.*, et al.* (2018). Development of clinical-stage human
1053 monoclonal antibodies that treat advanced Ebola virus disease in non-human primates. J Infect
1054 Dis.

1055 Pettersen, E.F., Goddard, T.D., Huang, C.C., Couch, G.S., Greenblatt, D.M., Meng, E.C., and
1056 Ferrin, T.E. (2004). UCSF Chimera--a visualization system for exploratory research and
1057 analysis. J Comput Chem *25*, 1605-1612.

1058 Punjani, A., Rubinstein, J.L., Fleet, D.J., and Brubaker, M.A. (2017). cryoSPARC: algorithms
1059 for rapid unsupervised cryo-EM structure determination. Nat Methods *14*, 290-296.

1060 Qiu, X., Alimonti, J.B., Melito, P.L., Fernando, L., Stroher, U., and Jones, S.M. (2011).
1061 Characterization of Zaire ebolavirus glycoprotein-specific monoclonal antibodies. Clin Immunol
1062 *141*, 218-227.

1063 Qiu, X., Fernando, L., Melito, P.L., Audet, J., Feldmann, H., Kobinger, G., Alimonti, J.B., and
1064 Jones, S.M. (2012). Ebola GP-specific monoclonal antibodies protect mice and guinea pigs from
1065 lethal Ebola virus infection. PLoS Negl Trop Dis *6*, e1575.

1066 Qiu, X., Wong, G., Audet, J., Bello, A., Fernando, L., Alimonti, J.B., Fausther-Bovendo, H.,
1067 Wei, H., Aviles, J., Hiatt, E.*, et al.* (2014). Reversion of advanced Ebola virus disease in
1068 nonhuman primates with ZMapp. Nature *514*, 47-53.

1069 Saphire, E.O., Schendel, S.L., Fusco, M.L., Gangavarapu, K., Gunn, B.M., Wec, A.Z.,
1070 Halfmann, P.J., Brannan, J.M., Herbert, A.S., Qiu, X.*, et al.* (2018a). Systematic Analysis of
1071 Monoclonal Antibodies against Ebola Virus GP Defines Features that Contribute to Protection.
1072 Cell *174*, 938-952 e913.

1073 Saphire, E.O., Schendel, S.L., Gunn, B.M., Milligan, J.C., and Alter, G. (2018b). Antibody-
1074 mediated protection against Ebola virus. Nat Immunol *19*, 1169-1178.

1075 Steichen, J.M., Kulp, D.W., Tokatlian, T., Escolano, A., Dosenovic, P., Stanfield, R.L., McCoy,
1076 L.E., Ozorowski, G., Hu, X., Kalyuzhniy, O.*, et al.* (2016). HIV Vaccine Design to Target
1077 Germline Precursors of Glycan-Dependent Broadly Neutralizing Antibodies. Immunity *45*, 483-
1078 496.

1079 Steichen, J.M., Lin, Y.C., Havenar-Daughton, C., Pecetta, S., Ozorowski, G., Willis, J.R., Toy,
1080 L., Sok, D., Liguori, A., Kratochvil, S., *et al.* (2019). A generalized HIV vaccine design strategy
1081 for priming of broadly neutralizing antibody responses. Science *366*.

1082 Thornburg, N.J., Zhang, H., Bangaru, S., Sapparapu, G., Kose, N., Lampley, R.M., Bombardi,
1083 R.G., Yu, Y., Graham, S., Branchizio, A., *et al.* (2016). H7N9 influenza virus neutralizing
1084 antibodies that possess few somatic mutations. J Clin Invest *126*, 1482-1494.

1085 Tran, E.E., Simmons, J.A., Bartesaghi, A., Shoemaker, C.J., Nelson, E., White, J.M., and
1086 Subramaniam, S. (2014). Spatial localization of the Ebola virus glycoprotein mucin-like domain
1087 determined by cryo-electron tomography. J Virol *88*, 10958-10962.

1088 Valley, C.C., Cembran, A., Perlmutter, J.D., Lewis, A.K., Labello, N.P., Gao, J., and Sachs, J.N.
1089 (2012). The methionine-aromatic motif plays a unique role in stabilizing protein structure. J Biol
1090 Chem *287*, 34979-34991.

1091 Wec, A.Z., Herbert, A.S., Murin, C.D., Nyakatura, E.K., Abelson, D.M., Fels, J.M., He, S.,
1092 James, R.M., de La Vega, M.A., Zhu, W., *et al.* (2017). Antibodies from a Human Survivor
1093 Define Sites of Vulnerability for Broad Protection against Ebolaviruses. Cell *169*, 878-890 e815.

1094 West, B.R., Moyer, C.L., King, L.B., Fusco, M.L., Milligan, J.C., Hui, S., and Saphire, E.O.
1095 (2018). Structural Basis of Pan-Ebolavirus Neutralization by a Human Antibody against a
1096 Conserved, yet Cryptic Epitope. MBio *9*.

1097 West, B.R., Wec, A.Z., Moyer, C.L., Fusco, M.L., Ilinykh, P.A., Huang, K., Wirchnianski, A.S.,
1098 James, R.M., Herbert, A.S., Hui, S., *et al.* (2019). Structural basis of broad ebolavirus
1099 neutralization by a human survivor antibody. Nat Struct Mol Biol *26*, 204-212.

1100 Williamson, L.E., Flyak, A.I., Kose, N., Bombardi, R., Branchizio, A., Reddy, S., Davidson, E.,
1101 Doranz, B.J., Fusco, M.L., Saphire, E.O., *et al.* (2019). Early Human B Cell Response to Ebola
1102 Virus in Four U.S. Survivors of Infection. J Virol *93*.

1103 Wilson, J.A., Hevey, M., Bakken, R., Guest, S., Bray, M., Schmaljohn, A.L., and Hart, M.K.
1104 (2000). Epitopes involved in antibody-mediated protection from Ebola virus. Science *287*, 1664-
1105 1666.

1106 Yu, X., McGraw, P.A., House, F.S., and Crowe, J.E., Jr. (2008). An optimized electrofusion-
1107 based protocol for generating virus-specific human monoclonal antibodies. J Immunol Methods
1108 *336*, 142-151.

1109 Yuan, M., Cottrell, C.A., Ozorowski, G., van Gils, M.J., Kumar, S., Wu, N.C., Sarkar, A.,
1110 Torres, J.L., de Val, N., Copps, J., *et al.* (2019). Conformational Plasticity in the HIV-1 Fusion
1111 Peptide Facilitates Recognition by Broadly Neutralizing Antibodies. Cell Host Microbe *25*, 873-
1112 883 e875.

1113 Zeitlin, L., Pettitt, J., Scully, C., Bohorova, N., Kim, D., Pauly, M., Hiatt, A., Ngo, L.,
1114 Steinkellner, H., Whaley, K.J., *et al.* (2011). Enhanced potency of a fucose-free monoclonal
1115 antibody being developed as an Ebola virus immunoprotectant. Proc Natl Acad Sci U S A *108*,
1116 20690-20694.

1117 Zhang, K. (2016). Gctf: Real-time CTF determination and correction. J Struct Biol *193*, 1-12.

1118 Zhao, X., Howell, K.A., He, S., Brannan, J.M., Wec, A.Z., Davidson, E., Turner, H.L., Chiang,
1119 C.I., Lei, L., Fels, J.M., *et al.* (2017). Immunization-Elicited Broadly Protective Antibody
1120 Reveals Ebolavirus Fusion Loop as a Site of Vulnerability. Cell *169*, 891-904 e815.

1121 Zhao, Y., Ren, J., Harlos, K., Jones, D.M., Zeltina, A., Bowden, T.A., Padilla-Parra, S., Fry,
1122 E.E., and Stuart, D.I. (2016). Toremifene interacts with and destabilizes the Ebola virus
1123 glycoprotein. Nature *535*, 169-172.

1124 Zheng, S.Q., Palovcak, E., Armache, J.P., Verba, K.A., Cheng, Y., and Agard, D.A. (2017).
1125 MotionCor2: anisotropic correction of beam-induced motion for improved cryo-electron
1126 microscopy. Nat Methods *14*, 331-332.

1127 Zivanov, J., Nakane, T., Forsberg, B.O., Kimanius, D., Hagen, W.J., Lindahl, E., and Scheres,
1128 S.H. (2018). New tools for automated high-resolution cryo-EM structure determination in
1129 RELION-3. Elife *7*.

1130 Zost, S.J., Gilchuk, P., Case, J.B., Binshtein, E., Chen, R.E., Nkolola, J.P., Schafer, A., Reidy,
1131 J.X., Trivette, A., Nargi, R.S.*, et al.* (2020). Potently neutralizing and protective human
1132 antibodies against SARS-CoV-2. Nature *584*, 443-449.
1133

Figure 1

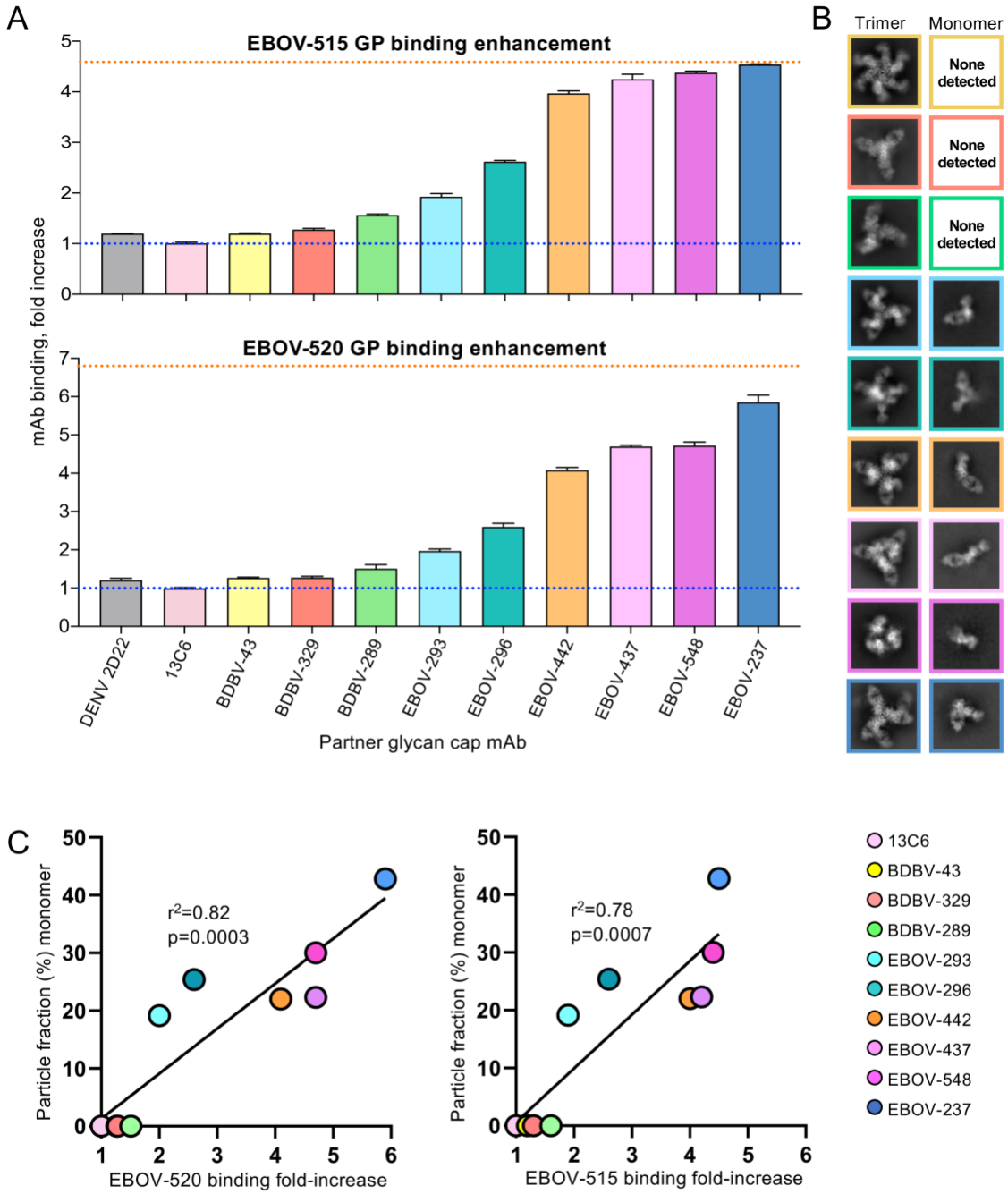

Figure 2

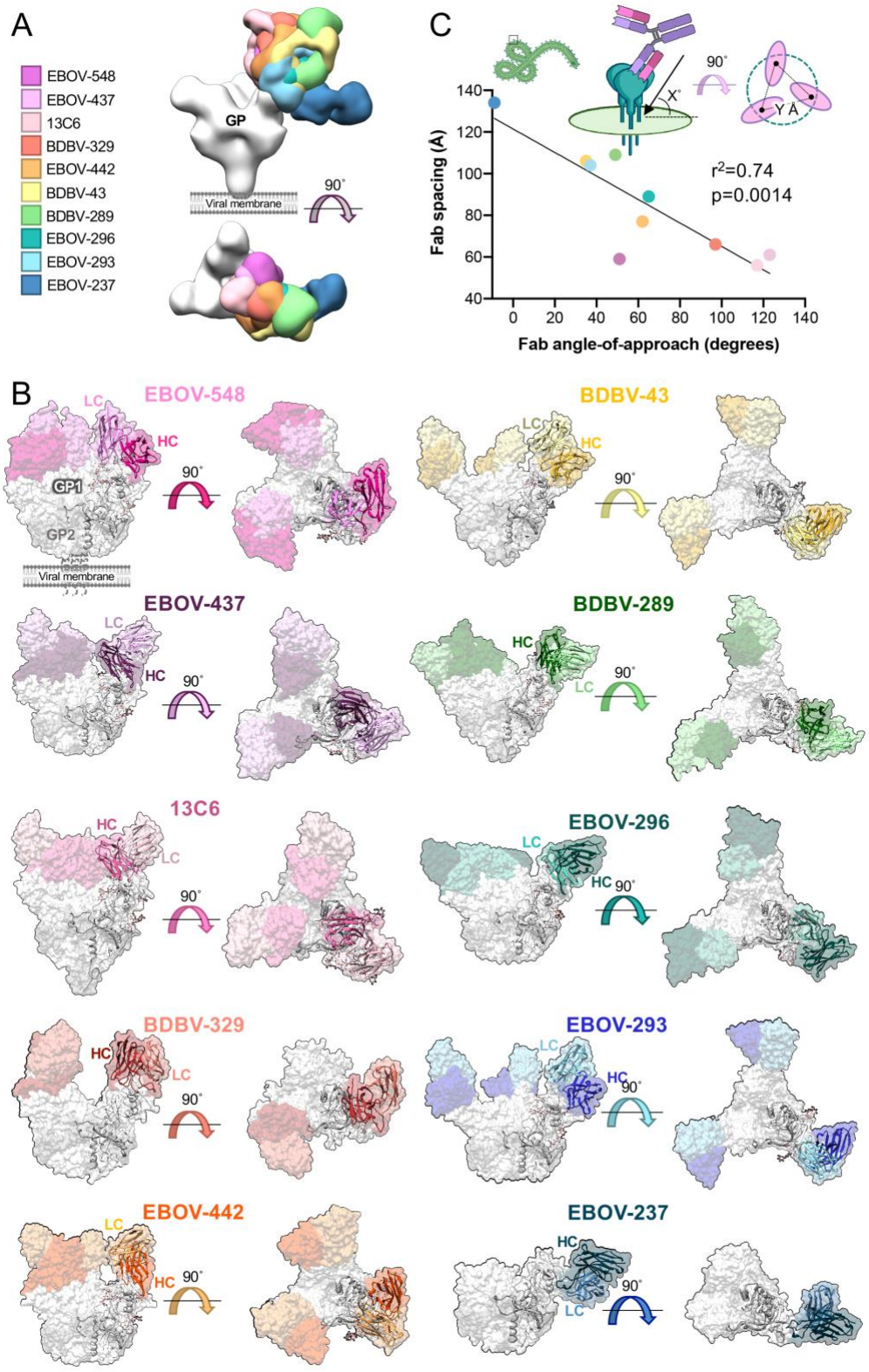

Figure 3

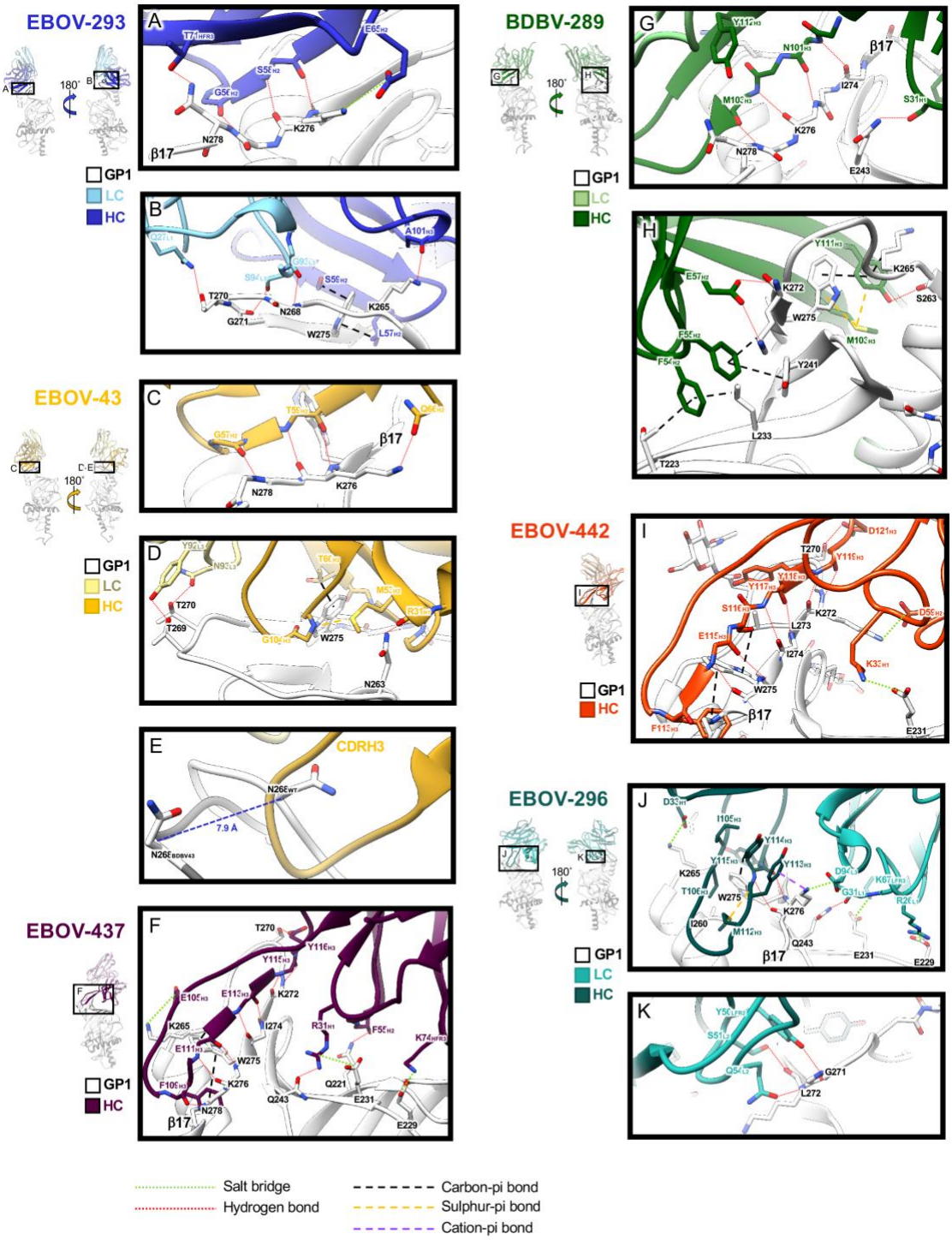

Figure 4

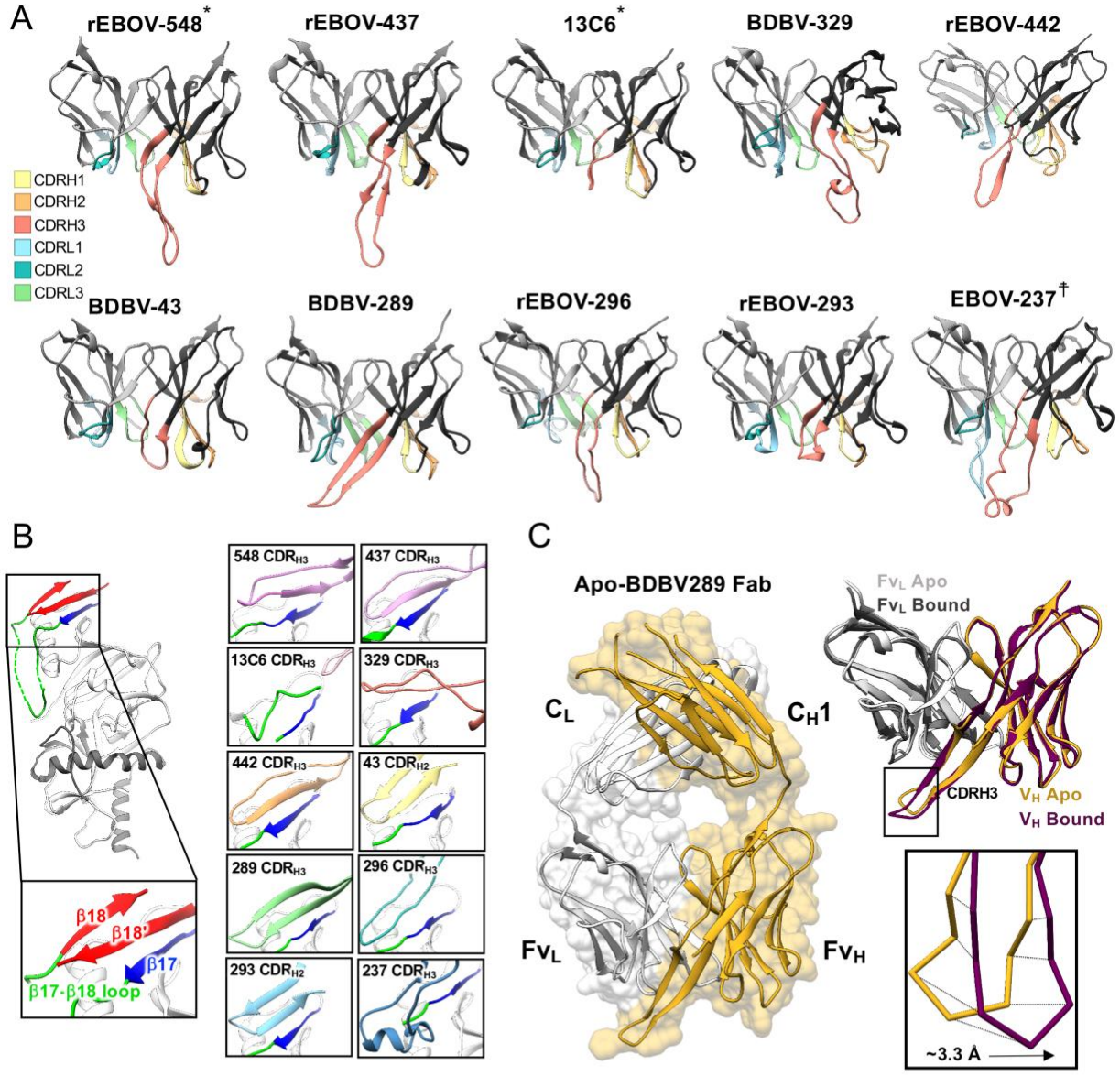

Figure 5

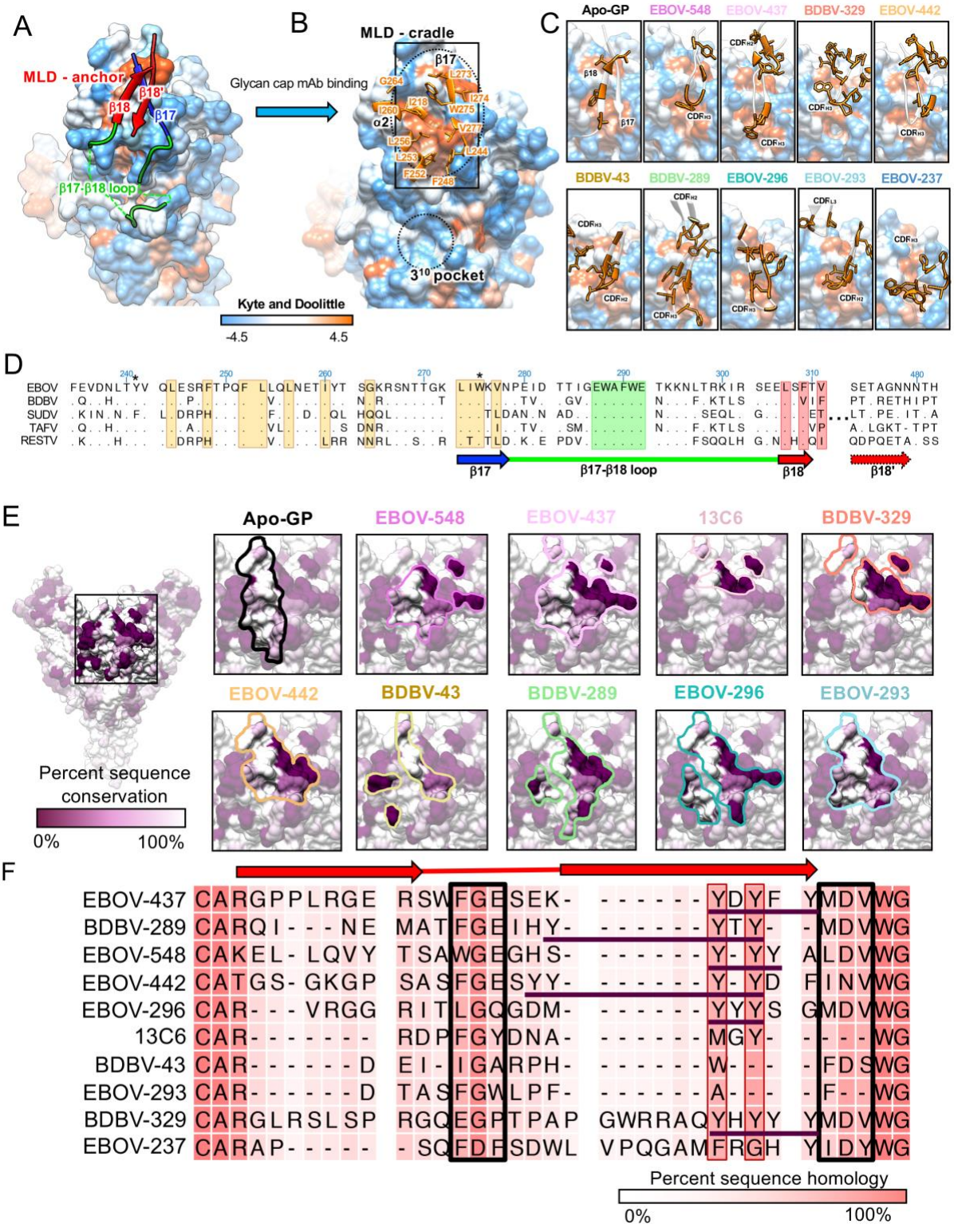

Figure 6

A

Antibody	IC_{50} (μg/mL)	IC_{90} (μg/mL)
EBOV-237	24.3	>60
EBOV-548	11.8	41.7
EBOV-437	2.3	6.6
EBOV-442	0.4	2.2
EBOV-296	8.5	19.3
EBOV-293	7.5	20.1
EBOV-289	5.0	30.2
EBOV-329	NA	NA
13C6	7.2	23.7
2G4	>60	NA
2D22	NA	NA

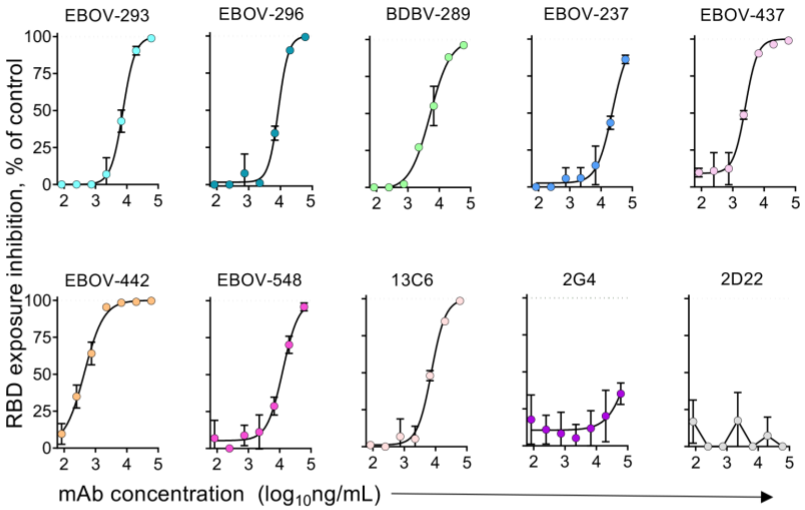

B